Assessing impacts of tidal power lagoons of a consistent design

Assessing impacts of tidal power lagoons of a consistent design

Lucas Mackie[a,*], Stephan C. Kramer[a], Matthew D. Piggott[a], Athanasios Angeloudis[b]

[a]*Department of Earth Science & Engineering, Imperial College London, UK*
[b]*School of Engineering, Institute for Infrastructure and the Environment, University of Edinburgh, UK*

Abstract

Tidal power lagoons have the potential to provide a reliable and long-term source of renewable power. The construction of tidal lagoons will impact the tidal conditions and hydrodynamics of the surrounding coastal system. Impact assessments in the academic literature have generally investigated working proposals from industry of various shapes and sizes. As such, differences between the impacts arising from considered power plants in varying sites are in part influenced by the individual scheme characteristics, potentially masking the influence of site-specific factors. In this study, scheme design consistency is maintained, providing a basis to focus solely on the merits of the selected locations with regards to any associated impacts. The tidal power lagoons are located in the Bristol Channel and Irish Sea, two distinct but tidally connected regions on the British coastline with contrasting marine environment characteristics. Results indicate that the more constrained geometry of the Bristol Channel contributes to higher individual and cumulative impacts than potential developments in the Irish Sea. This is in part facilitated by the higher degree of blockage introduced by tidal lagoon developments in the Bristol Channel. Furthermore, far-field impacts are found to be less pronounced in comparison to predictions reported in tidal barrage modelling studies.

Keywords: Tidal range energy, marine energy, hydrodynamic impact, resource assessment, consistent design

1. Introduction

Tidal range power plants are a marine-based source of hydroelectric power. They consist of coastal impoundments which delay tidal phasing between multiple marine water bodies. In coastally-attached designs, the impoundment perimeter is formed by a combination of the coastline and an embankment. Turbines, sluices and their housings are incorporated within sections of the embankment, facilitating head differences that enable periodic conversion of potential energy to electricity [1]. Such tidal range technology is well-established, but current worldwide installed capacity remains low La Rance Tidal Power Station (240 MW) in France and the Lake Sihwa Tidal Power Station (254 MW) in South Korea are among just a handful of

*Corresponding author
Email address: l.mackie18@imperial.ac.uk (Lucas Mackie)

operational schemes globally [2]. A first approximation to the tidal range energy resource magnitude E (J) demonstrates its proportionality to both the wetted surface area of the enclosed impoundment A_w (m^2) and the tidal range R (m) via $E \propto A_\mathrm{w} R^2$ [3]. Typical power plant designs therefore maximise energy output E by siting a large-scale impoundment A_w in a location exhibiting a high tidal range R.

The west coast of Great Britain contains among the highest tidal ranges worldwide [4]. Situated here is the Bristol Channel, which resonates with semi-diurnal tidal constituents, amplifying tidal elevations already magnified by the channel's funnel-like shape [5]. This fosters tidal ranges regularly exceeding 12 m. Meanwhile, extensive sections of the Irish Sea coastline to the north of Wales exhibit tidal ranges from 6 to 10 m [6]. Proposals to harness this abundant, low-carbon energy source through tidal range power plants have been considered in these two regions for many decades [7]. Tidal range power plants offer resource predictability and operational flexibility not afforded by other common renewable energy generators [8, 9, 10]. There is a body of research investigating and assessing economical tidal range energy design, implementation and operation in a UK-based setting [11, 12, 13, 14, 15].

The presence of a large-scale coastal structure which intermittently funnels substantial volumes of water will invariably impact the local and regional marine environment. Notable alterations in both water level and intertidal zone area occur within the tidal power plant impoundment. These can also be observed at near- and far-field locations outside of the impoundment, although generally to a lesser extent [16, 17, 18, 19]. Meanwhile, the redirection of flow can result in significant changes to water velocity [6, 16] and increases in vorticity [20]. These effects can impact marine ecology, sediment dynamics and water quality, as well as regional coastal infrastructure [21, 22, 23]. Numerical models are employed to predict tidal power plant impacts and facilitate mitigation strategies.

The most economical tidal power plant designs typically consist of a barrage spanning an estuary. In these designs, the impoundment perimeter is predominantly composed of estuarine coastline. Numerous publications report the extensive and prominent impacts predicted to arise from proposed tidal barrages along the west coast of Great Britain [5, 11, 18, 23, 24, 25]. The associated environmental consequences are a concern to stakeholders, including the general public [26]. As such, many recent proposals have favoured a tidal lagoon design, where the embankment forms either the majority or entirety of the impoundment perimeter to avoid the complete blockage of estuarine ecosystems. It is generally established that there is a reduced environmental impact induced by tidal lagoons in comparison to tidal barrages [2, 4, 27, 28]. There is, however, still a need to better understand the local, regional and far-field impact of tidal power lagoons.

Both impoundment design and the marine environment surrounding potential development locations are influential in dictating the nature of the impacts that may arise from specific tidal lagoon structures. Modelling-based tidal lagoon impact assessments have thus far typically been conducted in relation to specific industrial proposals and designs [5, 27, 28]. Few studies have investigated tidal lagoon designs not proposed

by industry [6, 17], but in those cases, little emphasis is reported on design rationale. Angeloudis et al. [6] assessed the impact of four adjacent but differently sized and shaped tidal lagoons operating simultaneously in the same British west coast region. The coastal tidal lagoons investigated by Cornett et al. [17] also varied in their impoundment design. In these earlier studies, simultaneous variations of both design and location makes drawing conclusions extremely challenging, if not speculative. This study instead focuses specifically on assessing the locations where tidal power plants are implemented. In maintaining design shape and size consistency, effects associated with deviating designs are minimised. As such, differences in predicted impacts between candidate locations become solely a product of physical marine environment attributes. A revised understanding of how local and regional marine environment factors – such as coastline geometry, bathymetry and tidal conditions – influence the potential impact of tidal lagoons could prove valuable to preliminary site selection for future projects.

The siting flexibility afforded by tidal lagoons permits the development of multiple schemes within the same estuary or geographical region. Quantifying the cumulative impact of multiple tidal power lagoons is an important consideration [6, 17]. An understanding of how plants interact will influence the siting and design of successively constructed schemes. In addition, impacts on the surrounding tidal range energy resource, that could be potentially exploited by future schemes, need to be considered. Planning and policy implications regarding energy resource impact have been discussed in relation to wind energy [29] and tidal stream energy [30]. A similar framework for managing tidal power lagoon co-location requires insight into the influence of the marine environment on tidal range resource impact. In applying a consistent design, the nature of impacts arising from the implementation of multiple tidal power lagoons can be investigated in a robust manner.

The structure of this study is as follows:

- A multi-scale, depth-averaged model characterising tidal conditions along the west coast of Great Britain is constructed and validated.
- Seven candidate locations for the development of tidal energy lagoons are selected across coastal areas in the Bristol Channel and Irish Sea regions.
- A consistent design is applied for all tidal lagoons in order to prevent design-specific elements influencing impact magnitude. Notably, the same impoundment surface plan area and shape is prescribed.
- Metrics for tidal conditions, hydrodynamics, bed shear stress and tidal energy resource are extracted from outputs of both the ambient model and configurations of the model containing tidal lagoons.
- Impacts associated with the implemented tidal lagoon developments are quantified and discussed.

2. Methodology

2.1. Hydrodynamic modelling

This study employs the coastal and estuarine flow model, *Thetis* [1] [31, 32] which is built using *Firedrake*, a finite element based Partial Differential Equation (PDE) solver framework [33]. The setup described here is similar to other studies which employ *Thetis* for tidal range energy assessment [10, 14, 15, 23]. For this work, *Thetis* is configured to solve the non-conservative form of the shallow-water equations:

$$\frac{\partial \eta}{\partial t} + \nabla \cdot (D\mathbf{u}) = 0, \tag{1}$$

$$\frac{\partial \mathbf{u}}{\partial t} + \mathbf{u} \cdot \nabla \mathbf{u} - \nu \nabla^2 \mathbf{u} + f\mathbf{u}^{\perp} + g\nabla\eta = -\frac{\boldsymbol{\tau}_{\mathrm{b}}}{\rho D}. \tag{2}$$

These equations consider the depth-averaged velocity vector $\mathbf{u}$ (ms^{-1}) (consisting of horizontal components u and v), free surface water elevation η (m), fluid density ρ (kgm^{-3}), total water depth D (m), kinematic viscosity ν ($\mathrm{m}^2\mathrm{s}^{-1}$), bed shear stress $\boldsymbol{\tau}_{\mathrm{b}}$ ($\mathrm{kgm}^{-1}\mathrm{s}^{-2}$) and Coriolis effects represented by $f\mathbf{u}^{\perp}$. In the latter, $f = 2\Omega\sin(\zeta)$ (Ω is the angular frequency of the Earth's rotation and ζ the latitude) and $\mathbf{u}^{\perp}$ indicates the velocity vector rotated anti-clockwise over 90°. Manning's n ($\mathrm{sm}^{-1/3}$) formulation is employed to calculate $\boldsymbol{\tau}_{\mathrm{b}}$:

$$\frac{\boldsymbol{\tau}_{\mathrm{b}}}{\rho} = gn^2 \frac{|u|\mathbf{u}}{D^{\frac{1}{3}}}. \tag{3}$$

Furthermore, a wetting and drying algorithm described in Kärnä et al. [34] is used to represent intertidal zones. This formulation ensures consistently positive total water depth through a modified bathymetry $\tilde{h} = h + f(D)$, where $f(D)$ is defined as:

$$f(D) = \frac{1}{2}\left(\sqrt{D^2 + \alpha^2} - D\right). \tag{4}$$

A value of the constant $\alpha = 0.5$ m is applied in this study which is consistent with previous studies.

The model employs the velocity-pressure finite element pair $\mathbb{P}1_{\mathrm{DG}}-\mathbb{P}1_{\mathrm{DG}}$ as part of a piecewise-linear discontinuous Galerkin finite element discretisation (DG-FEM). Temporal discretisation is via a semi-implicit Crank–Nicolson timestepping approach. A constant timestep $\Delta t = 100$ s is employed; this value was established following a sensitivity analysis.

[1] `http://thetisproject.org/`

2.2. Modelling tidal energy lagoons

0D and 2D representations of tidal power lagoon operation are often employed in tidal range energy modelling assessments [13]. Both model types are applied in this study, the setup and solutions of which are discussed below:

1. *0D operation model:* A 0D model has been applied in similar works for its computational efficiency [10, 14, 35, 36]. In this approach, tidal elevations outside the tidal lagoon impoundment η_{o} (m) are harmonically reconstructed from the ambient model at nearby sampling locations. Tidal elevations inside the tidal lagoon impoundment η_{i} (m) are then iteratively determined via an inverse finite difference solver, from which flow rate through the hydraulic structures can be calculated [10]. Power output is subsequently determined via turbine parameterisations [9, 12]. The limitations of 0D tidal range power modelling are well-documented [13] – a characterisation of hydrodynamics is required for impact quantification and higher accuracy power output estimations.
2. *2D hydrodynamic model:* The representation of tidal energy lagoons in the 2D model (Section 2.1) employs a technique of domain decomposition, as described by Angeloudis et al. [6]. Each tidal lagoon impoundment is implemented as a subdomain, connected to the main ocean domain via flux computations. The flux is calculated using the same turbine parameterisations as in the 0D model [10, 14]. Modelling the tidal lagoons this way allows the quantification of hydrodynamic and resource impact.

2.3. Plant operation and optimisation

The tidal power plants in this study all operate bi-directionally, generating electricity on both the ebb phase as the impoundment empties, and on the flood phase as the impoundment fills. In addition, pumping periods are implemented to increase impoundment elevation at high tide for ebb generation, and to reduce elevation at low tide for flood generation. This has been found to increase the energy output of prospective schemes [37].

Certain design and operational characteristics of the tidal power plants are optimised. This ensures a fair comparison across the sites through targeting economical exploitation of the tidal resource. The optimisation process is carried out on each scheme individually, making use of the 0D model to simulate tidal power plant operation. A simple homology global optimisation (SHGO) [2] algorithm is utilised [38, 39]. A global optimum of the vector of design parameters $\mathbf{x}$ is sought. This vector contains the turbine number (N_{T}) and 'holding' periods on the ebb ($t_{\mathrm{h,e}}$) and flood tide ($t_{\mathrm{h,f}}$). The number of sluice gates is given by $N_{\mathrm{S}} = N_{\mathrm{T}}/2$, an empirical relationship established in the literature [40]. As N_{S} is not a variable which greatly impacts

[2] `https://stefan-endres.github.io/shgo/`

the power output of bi-directional tidal power plants for the applied turbine parameterisation [9, 12], an economic model would be required to determine its optimum value.

Holding periods indicate the duration for which water is restricted from passing through the turbines following high and low tide, thus directly affecting the head difference driving turbine generation. These periods (contained in $\mathbf{x}$) therefore have a governing influence on the magnitude, duration and timing of the scheme power output: $P(\mathbf{x}, t)$. Previous studies have optimised these holding periods by either fixing the values in time, or by allowing variation between tidal cycles [10, 14, 15]. For efficiency, fixed-duration holding periods are herein established for each tidal power plant. Iterations of the optimisation span $n_\mathrm{c} = 200$ tidal cycles. Each cycle lasts $T_{\mathrm{M}_2} = 12.42$ h, as per the dominant lunar constituent M_2.

The optimisation process employs multiple objective functions ((7), (8) and (9)), which jointly consider both the overall energy generated by the scheme and the capacity factor of individual turbines. The decision variables in $\mathbf{x}$ are bound by individual upper and lower limits $\mathbf{x}_\mathrm{l} \leq \mathbf{x} \leq \mathbf{x}_\mathrm{u}$. At each iteration, energy output E (GWh) (6) is computed as a factor E_C of theoretical maximum energy output E_th (GWh) (5), given by $E_\mathrm{C} = E/E_\mathrm{th}$, where

$$E_\mathrm{th} = \sum_{i=1}^{n_\mathrm{c}} \frac{1}{2} \rho g \overline{A_\mathrm{w}} {H_\mathrm{i}}^2, \tag{5}$$

$$E = \int_{t=0}^{t=n_\mathrm{c} \times T_{\mathrm{M}_2}} P(\mathbf{x}, t)\, dt. \tag{6}$$

Equation (5) considers the mean wetted surface area $\overline{A_\mathrm{w}}$ (km^2), fluid density ρ (kgm^{-3}) and, at each tidal cycle i in n_c, the head difference either side of the embankment H_i (m). This theoretical assessment of energy output (5) considers $H_\mathrm{i} = R_\mathrm{i}$, where R_i is the tidal range at a given tidal cycle. In (6), time-dependent power output $P(\mathbf{x}, t)$ (GW) is integrated over the considered timeframe. Meanwhile, power capacity factor P_C is related to the average operation power output $\overline{P}$ (GW) and the installed capacity of the tidal power plant P_I (GW) through $P_\mathrm{C} = \overline{P}/P_\mathrm{I}$.

Initially, the maximum values of E_C and P_C permitted by varying $\mathbf{x}$ are determined. The SHGO algorithm sequentially optimises $\max(E_\mathrm{C})$ using the objective function (7), and $\max(P_\mathrm{C})$ using (8).

$$\begin{aligned} \max(E_\mathrm{C}) = \max_{\mathbf{x}} \quad & \frac{E(\mathbf{x})}{E_\mathrm{th}(H)} \\ \text{subject to} \quad & \mathbf{x}_\mathrm{l} \leq \mathbf{x} \leq \mathbf{x}_\mathrm{u} \end{aligned} \tag{7}$$

$$\begin{aligned} \max(P_\mathrm{C}) = \max_{\mathbf{x}} \quad & \frac{\overline{P}(\mathbf{x})}{P_\mathrm{I}(\mathbf{x})} \\ \text{subject to} \quad & \mathbf{x}_\mathrm{l} \leq \mathbf{x} \leq \mathbf{x}_\mathrm{u} \end{aligned} \tag{8}$$

The second stage of the optimisation process considers the objective function (9), which normalises E_C and P_C against their respective maximums $\max(E_C)$ and $\max(P_C)$:

$$\begin{aligned} \max_{\mathbf{x}} \quad & a\frac{E_C(\mathbf{x})}{\max(E_C)} + b\frac{P_C(\mathbf{x})}{\max(P_C)} \\ \text{subject to} \quad & \mathbf{x}_l \leq \mathbf{x} \leq \mathbf{x}_u \end{aligned} \tag{9}$$

The two elements of this function are weighted by their importance to scheme design. Values of $a = 0.55$ and $b = 0.45$ reflect the prioritisation of maximising energy output, whilst ensuring sufficient utilisation of the installed capacity. These weightings (a, b) were selected following a preliminary sensitivity study, but should be practically defined according to an economic analysis of the scheme components.

2.4. Quantifying impact

Model solution outputs of free surface elevation η (m) and depth-averaged velocity components u, v (ms^{-1}) are interpolated onto either transects or regular grids at 500 s intervals. The impact of tidal power lagoons is determined by calculating the difference (Δ) in several indicative metrics between the ambient model and configurations of the model including tidal power lagoons:

1. *Harmonic tidal constituents:* The Python library *Uptide* [3] is used to perform harmonic analysis of free surface elevation η, from which tidal constituent amplitude α (m) and phase ϕ (°) can be determined.
2. *Intertidal zones:* Total water depth D (m) can be calculated by considering bathymetry h (m) via $D = \eta + h$. By establishing the transient location of $D = 0$ (the intertidal boundary), the evolution of 'wet' A_w and 'dry' A_d surface areas (both km^2) can be determined over time.
3. *Volume Flux:* Flux, Q_T ($\mathrm{m}^3\mathrm{s}^{-1}$) can be calculated through transects using u, v outputs and D. By sequentially integrating Q_T over individual tidal cycles ($t_c = 12.42$ h), the total volume exchange in m^3 is found via $V_T = \int_{t=i\times t_c}^{t=(i+1)\times t_c} Q(D,u,v)dt$, where i indicates the index of the tidal cycle in question.
4. *Stratification:* The Simpson Hunter Index (SHI) [41] is employed as a parameter for representing stratification in depth averaged coastal models: $\mathrm{SHI} = \log_{10}(D/|\mathbf{u}|^3)$. Lower SHI indicates well-mixed conditions, up to the critical value of 2.7 ± 0.3 $\mathrm{m}^{-2}\mathrm{s}^3$ which indicates the water column changing to stratified flow.
5. *Bed shear stress*: Manning's equation (3) is employed to determine bed shear stress $\boldsymbol{\tau}_b$ ($\mathrm{kgm}^{-1}\mathrm{s}^{-2}$), from which bed shear stress magnitude $|\tau_b|$ ($\mathrm{kgm}^{-1}\mathrm{s}^{-2}$) is considered as a proxy for characterising morphodynamics.
6. *Tidal range energy resource*: The theoretical energy per unit area E_A (GWh km^{-2}) over a given simulation period can be determined by adapting (5): $E_A = \sum_{i=1}^{n_c} \frac{1}{2}\rho g {H_i}^2$. E_A is here temporally

[3] `https://github.com/stephankramer/uptide`

scaled over a full year to give $E_{\mathrm{A,yr}}$. Energy resource impact is also estimated by considering the difference in energy output predicted by the 2D tidal lagoon model configurations applying tidal lagoons individually and in combinations. Energy output E (GWh) over a period ≤ 60 days (the 2D simulation duration) can be determined directly from the turbine flux computations in the 2D models. Predictions of energy output for periods > 60 days can be scaled using the 0D model [10, 42]. For example, an estimation of annual energy output E_{yr} (365 days) from the 2D model is calculated by determining the ratio between equivalent 60 and 365 day simulation energy outputs of the 0D model. The 60 day energy output for the 2D model is then scaled by this same ratio. Scaling the 2D model energy outputs in this way, instead of directly by time, considers the fact that the simulation period selected for assessing hydrodynamics may not be representative of the chosen areas in terms of energy output. Moreover, as the focus is on relative assessment rather than calculating E_{yr} for a particular scheme, this is seen as sufficient. The method employed for establishing the simulation period is discussed in Section 3.2.

3. Case study preliminary steps

3.1. Site selection

Seven locations across two regions are selected for analysis in this study. They have been labelled based upon a nearby town, city or landmark: Swansea (SW), Cardiff (CA), Watchet (WA) in the Bristol Channel region, and Colwyn (CO), Liverpool (LI), Blackpool (BL) and Solway (SO) in the Irish Sea region. Each of these locations has been considered for tidal power plant development in research, industry and government contexts, as indicated in Table 1.

Table 1: Previous studies investigating the tidal power potential of the seven selected study locations.

Location \ Sector	Research	Industry	Government
Swansea (SW)	[10][1] [43][1] [44][1,2,3]	[45][3,4] [46][1,3]	[47][1,3] [48][1]
Cardiff (CA)	[10][1] [28][1,2]	[45][3,4]	[47][1,3] [48][1]
Watchet (WA)	[15][1,3] [49][1]	[50][1,3] [51][4]	[52][1] [48][1]
Colwyn (CO)	[6][1,2] [53][2] [24][2]	[54][4]	[47][1,3] [48][1]
Liverpool (LI)	[9][1] [11][1] [24][2]	[55][1,3] [56][4]	[47][1,3] [48][1]
Blackpool (BL)	[1][1,3] [11][1] [24][2]	[57][1,3]	[47][1,3] [48][1]
Solway (SO)	[11][1] [12][1] [24][2]	[57][1,3]	[47][1,3] [48][1]

Assessment type:

[1] Tidal energy resource
[2] Environmental impact
[3] Economics
[4] Promotional

3.2. Establishing representative tidal conditions

A total of 60 days plus spin-up are simulated in the 2D numerical models, encompassing the period of two lunar months. The simulation start time is selected by identifying a date at which representative tidal conditions occur in the model domain for this 60 day duration. Using the TPXO database [58], tidal constituent data ($M_2, S_2, N_2, K_2, O_1, Q_1, P_1, K_1$) are extracted at locations in 1) the Bristol Channel and 2) the Irish Sea (indicated in Table 2 and Fig. 1). A 20 year tidal signal $\eta(t)$ starting at 01/01/2000 is generated so as to allow harmonic reconstruction of the full 18.6 year lunar nodal cycle [59]. High Water Spring $\eta_{\mathrm{HWS}}(t)$, High Water Neap $\eta_{\mathrm{HWN}}(t)$, Low Water Neap $\eta_{\mathrm{LWN}}(t)$ and Low Water Spring $\eta_{\mathrm{LWS}}(t)$ time series [60] are determined, with values for each occurring roughly every 14 days. Relative difference (%) and absolute difference (m) from the 20 year mean of each time-series are then calculated (η_{MHWS}, η_{MHWN}, η_{MLWN}, η_{MLWS}). The time frame deemed most representative of typical conditions exhibits the lowest maximum of the 16 relative error values (i.e. eight relative errors per 28 day lunar cycle) which can be established over two full lunar months (roughly 56 days), starting from each η_{HWS} occurrence. An average of the equivalent absolute errors is also computed. Table 2 illustrates how 14/01/2002 is selected as a suitable start time for simulating 60 days of typical tidal conditions.

Table 2: Results of method for determining start date of 60 day period most representative of typical tides. Start dates are ranked according to the lowest maximum relative error between four consecutive High Water Spring η_{HWS}, High Water Neap η_{HWN}, Low Water Neap η_{LWN} and Low Water Spring η_{LWS} values and the equivalent means of the full 20 year tide signal (η_{MHWS}, η_{MHWN}, η_{MLWN}, η_{MLWS}). The average absolute error is also indicated.

Location	Lat., Lon. (°N, °E)	Rank	Date	Max. Relative Error (%)	Mean Absolute Error (m)
1) Bristol Channel	(51.39, −4.11)	#1	31/01/2002	15.14	0.319
		#2	**14/01/2002**	**15.14**	**0.338**
		#3	14/10/2011	15.77	0.349
		#4	17/07/2015	16.39	0.348
		#5	06/01/2015	16.43	0.324
2) Irish Sea	(53.74, −3.69)	**#1**	**14/01/2002**	**14.83**	**0.302**
		#2	13/10/2011	15.01	0.304
		#3	12/10/2007	15.06	0.260
		#4	03/08/2019	15.21	0.275
		#5	17/07/2019	15.21	0.307

3.3. Setting up the 2D model domain

The inclusion of tidal power plants in coastal models can result in hydrodynamic changes at both near- and far-field locations [17, 28]. The open boundaries of the model must be located sufficiently far enough from the structures themselves, such that the conditions imposed at these boundaries (which are calculated using external models which do not include the presence of any lagoons) are largely unaffected by the presence and

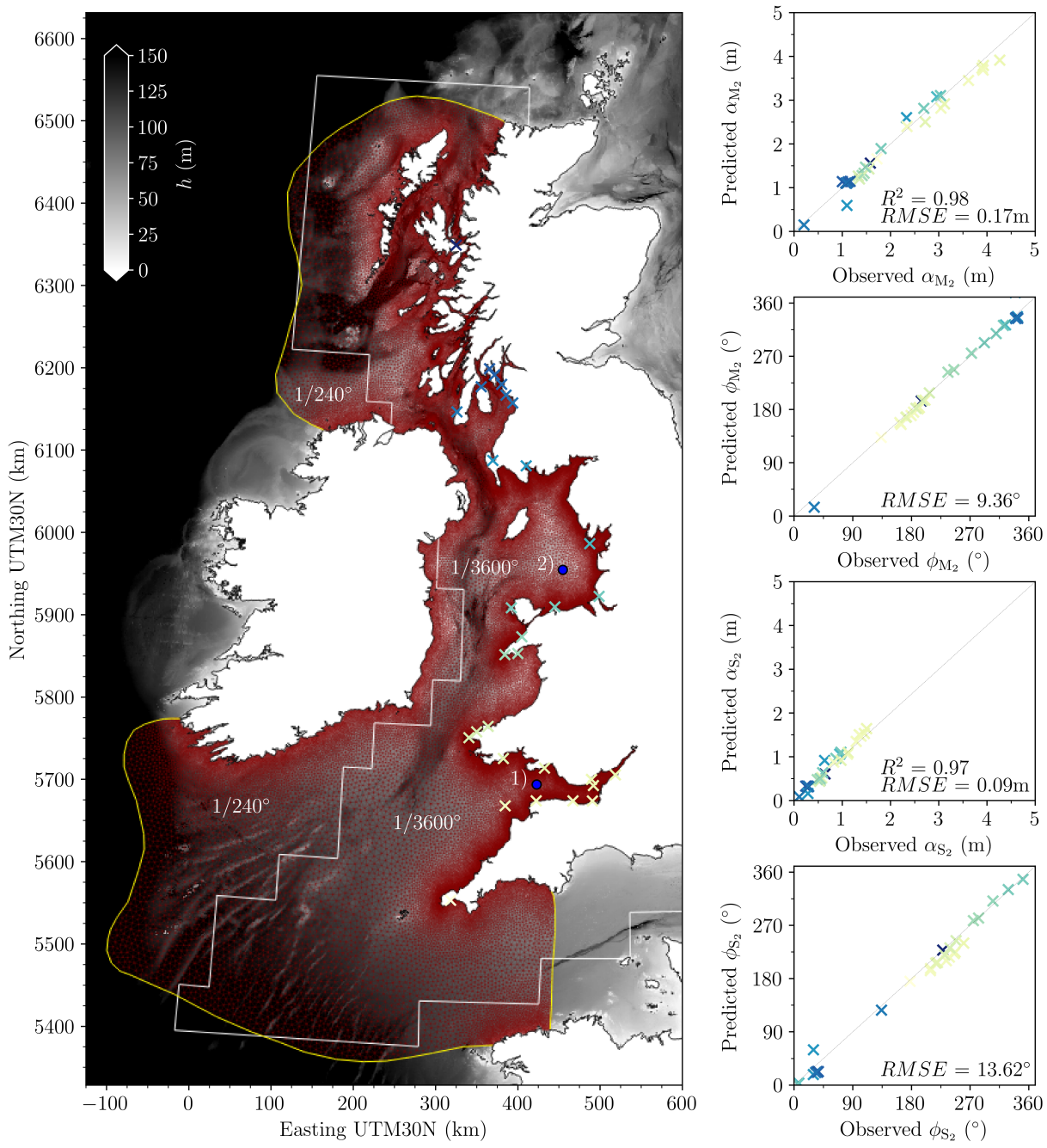

Figure 1: Computational mesh and domain including Irish Sea and Bristol Channel regions. Open ocean boundaries (shown in yellow) are located at the northern and southern west coast of Great Britain, and in the English Channel. Indicated 1/3600° and 1/240° bathymetry h (m) data are relative to lowest astronomical tide (LAT), but converted to mean water level (MWL) in the model; a white line separates the regions in which each data resolution is applied. Simulation duration is determined based on identification of the most typical tidal month at locations marked 1) and 2). Principal tidal constituents predicted by the model are compared to equivalent observations from BODC [61] identified by coloured crosses, with R^2 correlation coefficient and root mean squared error ($RMSE$) provided where relevant.

operation of the tidal power plants and thus still valid for model forcing. This is more commonly referred to as the 'open boundary problem', first reported by Garrett and Greenberg [62]. If the locations of the open boundaries are not adequately considered, this can have a major impact on the operation, hydrodynamic feedback and resource potential of modelled schemes [18]. The boundary locations applied by Mackie et al. [15] are considered as a baseline. Two domain extensions on the south coast are then modelled, both with and without tidal lagoons implemented. In Section A of the Supplementary Material, a sensitivity study of the open boundary problem [18] on the three tested domains is conducted, providing justification for the chosen configuration displayed in Fig. 1.

The following sections outline the composition of the 2D model, and are relevant to all considered model boundary configurations. However, indicated figures and quantities reflect the final chosen computational domain, which spans the length of Great Britain's west coast (Fig. 1).

3.3.1. Mesh and bathymetry

An unstructured mesh is generated using *qmesh* [4] [63, 64]. The mesh exhibits higher refinement along the coastline for accurate resolution of the coastline shape, and to assist the wetting and drying algorithm, which is sensitive to sharp resolution changes. A total of 70,947 nodes are present in the ambient model discretisation (without tidal lagoons).

Model bathymetry combines two datasets. The majority of the coastline and ocean domain interpolates $1/3600°$ resolution measurements (15–20 m in the model domain), obtained from Marine Digimap [65]. Where indicated on Fig. 1, $1/240°$ measurements (240–310 m) from GEBCO [66] are interpolated for the remainder of the ocean domain. These datasets are combined and converted to a UTM zone 30N (EPSG:32630) projection in the x- and y-direction. The $1/3600°$ Digimap bathymetry measurements (z-direction) are relative to lowest astronomical tide (LAT) and subsequently corrected to mean water level (MWL). This process makes use of tide constituent observations from TPXO [58]. The same eight constituents ($M_2, S_2, N_2, K_2, O_1, Q_1, P_1, K_1$) are used to force the model at the three open ocean boundaries. Freshwater inflows have not been included as they are unlikely to affect tidal dynamics.

3.3.2. Model calibration and validation

Calibration and validation of the ambient model utilises tide gauge measurements from the British Oceanographic Data Centre (BODC) [61]. Harmonic tidal constituents are extracted from the tide gauge station closest to each of the seven study locations. The model is then calibrated by adjusting constant values of Manning's coefficient n ($\mathrm{sm}^{-1/3}$) (3) and comparing observed harmonic constituents with equivalent predicted values, the latter extracted from detector locations in the numerical model (Fig. 2). A constant $n =$

[4] `https://www.qmesh.org/`

0.026 $\mathrm{sm}^{-1/3}$ is found to provide the best fit with measured amplitude α (m) and phase ϕ (^{o}) for the tidal constituents M_2, S_2, N_2 and K_2 in the seven tide gauge locations (Table 3).

Table 3: Free surface elevation η (m) is sampled at the seven case study locations. This provides the tidal range R (m) at each cycle over the 60 day period from 14/01/2002. Comparisons are then made between observed [Obs.] and predicted [Pred.] tidal constituent amplitude α (m) and phase ϕ (°) at the tide gauge locations nearest to the seven tidal lagoons. The tide gauge and elevation model sampling locations are both shown in Fig. 2.

	Swansea (SW)	**Cardiff (CA)**	**Watchet (WA)**	**Colwyn (CO)**	**Liverpool (LI)**	**Blackpool (BL)**	**Solway (SO)**
Tide Gauges:							
Name	Mumbles	Cardiff	Hinkley Point	Llandudno	Liverpool	Halfway Shoal	Creetown
Lat., Lon. (°N, °E)	(51.57, −3.98)	(51.45, −3.15)	(51.21, −3.13)	(53.33, −3.83)	(53.45, −3.02)	(54.03, −3.19)	(54.87, −4.40)
α_{M_2} (m) [Obs., Pred.]	[3.12, 2.91]	[3.92, 3.79]	[3.92, 3.69]	[2.69, 2.81]	[3.03, 3.10]	[2.96, 3.08]	[2.33, 2.60]
α_{S_2} (m) [Obs., Pred.]	[1.12, 1.10]	[1.46, 1.53]	[1.39, 1.47]	[0.87, 0.96]	[0.97, 1.10]	[0.94, 1.06]	[0.63, 0.92]
α_{N_2} (m) [Obs., Pred.]	[0.59, 0.56]	[0.72, 0.72]	[0.72, 0.70]	[0.52, 0.55]	[0.58, 0.59]	[0.57, 0.60]	[0.36, 0.49]
α_{K_2} (m) [Obs., Pred.]	[0.33, 0.33]	[0.40, 0.47]	[0.40, 0.46]	[0.25, 0.26]	[0.28, 0.30]	[0.27, 0.29]	[0.17, 0.25]
ϕ_{M_2} (^{o}) [Obs., Pred.]	[172.2, 167.3]	[192.0, 182.3]	[183.2, 175.5]	[309.9, 308.4]	[321.1, 322.2]	[324.3, 323.0]	[342.5, 337.0]
ϕ_{S_2} (^{o}) [Obs., Pred.]	[219.8, 207.2]	[247.0, 224.7]	[238.1, 216.4]	[351.1, 347.9]	[5.3, 2.2]	[7.3, 3.3]	[29.4, 17.8]
ϕ_{N_2} (^{o}) [Obs., Pred.]	[153.9, 152.2]	[174.0, 172.7]	[168.3, 164.1]	[285.9, 286.2]	[298.3, 302.9]	[300.6, 301.2]	[324.3, 317.3]
ϕ_{K_2} (^{o}) [Obs., Pred.]	[217.5, 214.1]	[247.0, 240.0]	[236.2, 230.1]	[349.9, 352.4]	[4.7, 14.2]	[6.0, 9.2]	[29.4, 31.1]
Tidal Resource:							
Lat., Lon. (°N, °E)	(51.49, −3.82)	(51.45, −3.06)	(51.23, −3.31)	(53.34, −3.63)	(53.43, −3.20)	(53.87, −3.12)	(54.79, −3.50)
$\overline{R}$ (m)	6.2	8.3	7.6	6.0	6.4	6.4	6.2
max(R) (m)	9.8	12.8	11.8	9.2	9.8	9.8	9.3
min(R) (m)	3.4	4.5	4.1	3.5	3.8	3.8	3.7
η_{max} (m)	5.1	6.9	6.3	4.6	4.9	4.9	4.8
η_{min} (m)	−4.7	−5.9	−5.5	−4.6	−4.8	−4.9	−4.5
(L)HAT (m)	(−)5.7	(−)8.0	(−)7.2	(−)5.4	(−)5.8	(−)5.7	(−)5.5

Model validation considers 30 tide gauge stations across the model domain [61]. Fig. 1 maps the tide gauges and provides root mean squared error ($RMSE$) between observed and predicted α and ϕ for the principal tidal constituents M_2 and S_2 (α_{M_2}, ϕ_{M_2}, α_{S_2}, ϕ_{S_2}). $RMSE$ of the circular phase metric ϕ considers the smallest difference between observed and predicted values. In addition, R^2 correlation coefficient is provided for validation of α values at the tide gauge locations. The calibrated results are competitive with recent results in the literature [67]. An indicator of tidal conditions characterised by the validated numerical model is provided in Table 3. Elevation time series $\eta(t)$ (m) are sampled at detector locations adjacent to the seven tidal lagoon locations (Table 3), from which tidal range R (m) can be calculated at each tidal cycle.

Both Table 3 and Fig. 1 suggest that the calibrated model slightly overestimates amplitudes in the Bristol Channel, whilst slightly underestimating amplitudes in the Irish Sea. This highlights potential limitations of applying a uniform bed roughness coefficient field. Warder and Piggott [68] report an optimal experiment design (OED) technique for estimating roughness coefficient parameter values distributed spatially in the

model. However, use of a constant Manning coefficient calibrates the model sufficiently for the aims of this study.

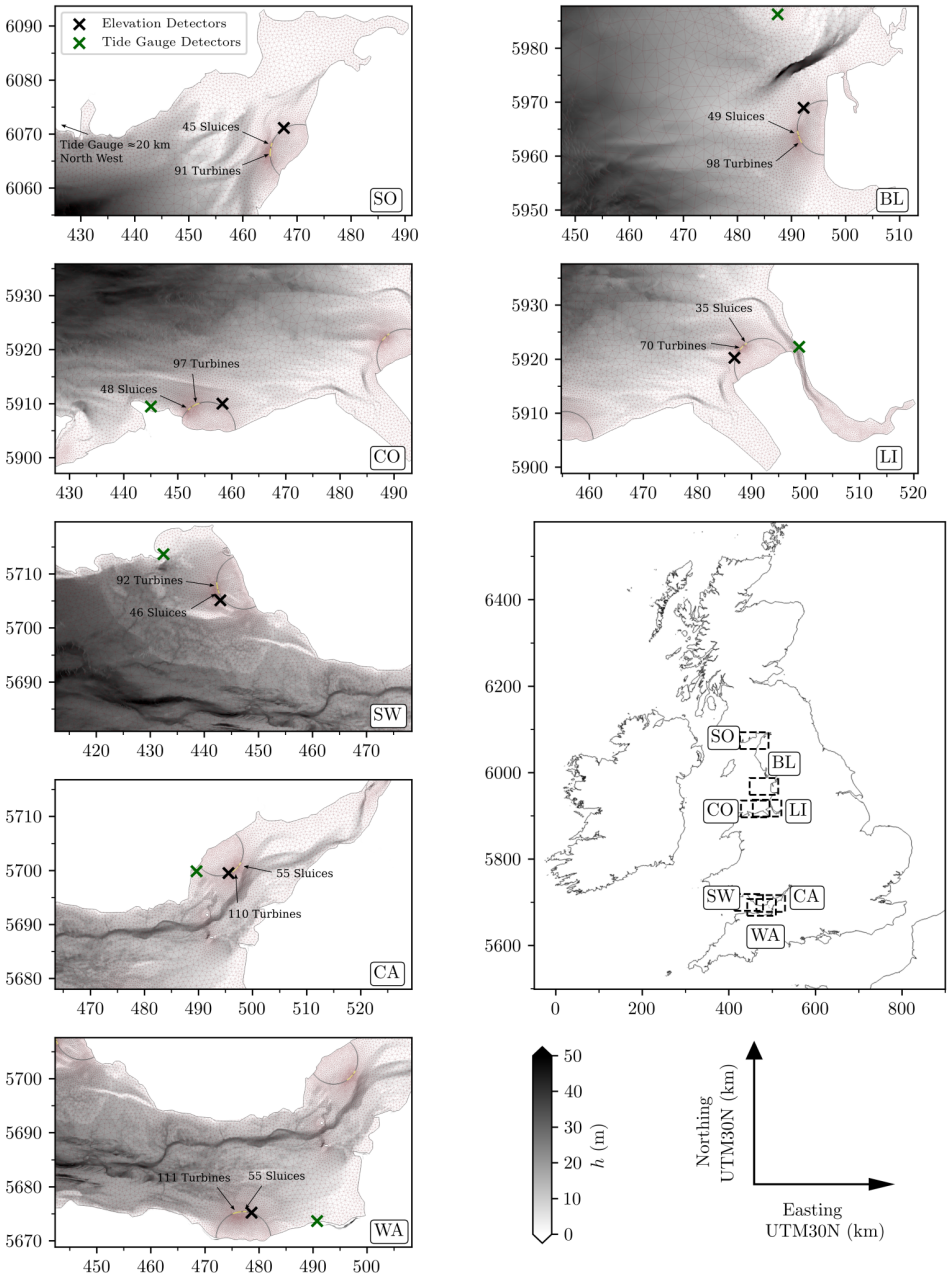

Figure 2: Map indicating the consistently designed tidal power lagoon impoundments at the seven locations selected for analysis. Only the 1/3600° resolution bathymetry h (m) measurements [65], relative to lowest astronomical tide (LAT), are displayed. Turbine and sluice locations and quantity are also indicated. Tide gauge and elevation detector locations are utilised for model validation and characterisation of tidal conditions in Table 3.

3.3.3. Tidal energy lagoon design

A consistent tidal power plant design strategy is applied, covering a semi-circular area from a circle centre positioned on the coastline. At highest astronomical tide (HAT), each scheme has a wetted surface plan area $\max(A_w) = 40$ km^2. Due to the irregular shape of the coastline, there exists slight variability in the length of the embankment and enclosed coastline between schemes. The selected impoundment design is approximately midway in size between the Swansea Bay and Cardiff tidal lagoons proposed by Tidal Lagoon Power [10]. The location, layout and surrounding bathymetry is displayed in Fig. 2. Fig. 3 indicates free surface elevations η_o (m) from the ambient model at elevation sampling locations (Fig. 2), and the relationship between impoundment elevation η_i (m) and wetted surface plan A_w (km^2).

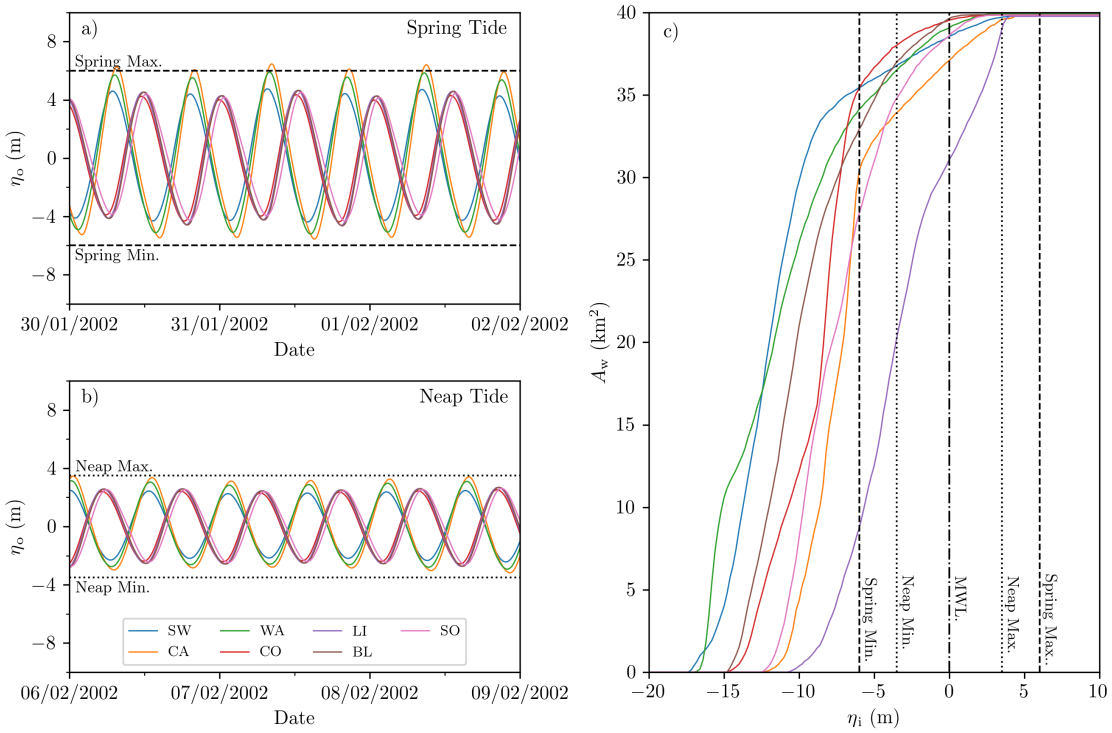

Figure 3: Free surface elevation η_o (m) sampled from the ambient model over a) spring and b) neap conditions at locations nearby the seven tidal lagoon impoundments (Fig. 2). c) indicates the relationship between impoundment elevation η_i (m) and wetted surface plan area A_w (km^2).

Operational characteristics of the individual tidal energy lagoons are established prior to their inclusion in the 2D model. At each tidal cycle, generation time before sluicing (defined in Harcourt et al. [14]) is fixed at $t_{g,e} = t_{g,f} = 3.5$ h in the ebb and flood phases, respectively, as in the study by Mackie et al. [69]. Pumping intervals are limited to $t_{p,e}$, $t_{p,f} < 0.5$ h, with these periods being curtailed if water elevations exceed local LAT or HAT values. Values of N_T, N_S, $t_{h,e}$ and $t_{h,f}$ are determined for each tidal power plant through the optimisation framework outlined in Section 2.3. The converged tidal power plant characteristics are provided

in Table 4.

Table 4: Scheme characteristics determined from the 0D model and optimisation, including wetted impoundment surface plan A_{w}, turbine number N_{T}, sluice number N_{S}, total hydraulic structure length L_{HS}, embankment length L_{E}, installed power capacity P_{I} and fixed holding periods $t_{\mathrm{h,e}}$, $t_{\mathrm{h,f}}$.

	Swansea (SW)	**Cardiff (CA)**	**Watchet (WA)**	**Colwyn (CO)**	**Liverpool (LI)**	**Blackpool (BL)**	**Solway (SO)**
$\overline{A_{\mathrm{w}}}$ (km^2)	38.4	36.8	38.6	39.3	30.5	39.0	38.2
max(A_{w}) (km^2)	39.8	39.8	39.9	39.9	39.8	39.9	39.9
min(A_{w}) (km^2)	36.1	30.7	34.6	37.1	13.3	35.0	32.5
N_{T}	92	110	111	97	70	98	91
N_{S}	46	55	55	48	35	49	45
L_{HS} (km)	2.1	2.5	2.5	2.2	1.6	2.2	2.0
L_{E} (km)	14.3	12.9	12.8	11.9	14.9	14.2	12.4
P_{I} (GW)	1.84	2.20	2.22	1.94	1.40	1.96	1.82
$t_{\mathrm{h,e}}$, $t_{\mathrm{h,f}}$ (h)	3.10, 3.40	2.63, 3.41	2.92, 3.27	3.25, 3.36	2.91, 3.49	2.94, 3.45	3.25, 3.36

Turbine capacity is 20 MW, diameter is 7.35 m and rated head 5m.

Sluices have a cross-sectional area of 150 m^2.

Individual hydraulic structures span 15 m of impoundment perimeter.

4. Results

4.1. Impact on harmonic tidal constituents

Ambient tidal conditions along the west coast of Great Britain are well-established in the literature [25, 67]. In Fig. 4, ambient model outputs are processed to display tidal amplitude α (m) and phase ϕ (°) for the principal semi-diurnal lunar constituent M_2: α_{M_2} and ϕ_{M_2}. The concentration of high amplitude areas surrounding the locations where tidal power plants are later added is evident. A significant phase difference can be observed between the two studied regions in the model: the Bristol Channel (BC) south of Wales and the Irish Sea (IS) north of Wales.

Fig. 5 and Fig. 6 illustrate changes (Δ) in tidal conditions to the ambient model induced by combinations of the seven candidate tidal energy lagoons. As well as predicting $\Delta\alpha_{\mathrm{M}_2}$ and $\Delta\phi_{\mathrm{M}_2}$ due to the presence of all seven tidal power plants together, results are also provided for when lagoons are only deployed in one of the Bristol Channel (BC) and the Irish Sea (IS). Where just BC tidal lagoons are included, a change of $-0.1 > \Delta\alpha_{\mathrm{M}_2} > -0.2$ m is present in the Bristol Channel. Smaller reductions in α_{M_2} are observed in far-field locations, including the Irish Sea. IS tidal lagoons trigger $\Delta\alpha_{\mathrm{M}_2}$ to a generally lower extent, with negligible impact in the Bristol Channel. Meanwhile, tidal phase in the model domain is altered to a greater degree as a result of tidal lagoons in the Irish Sea compared to tidal lagoons in the Bristol Channel. Overall, the impacts of tidal power lagoons in the two regions follow a linear cumulative relationship. Further evidence to support this hypothesis is provided in Section B in the Supplementary Material.

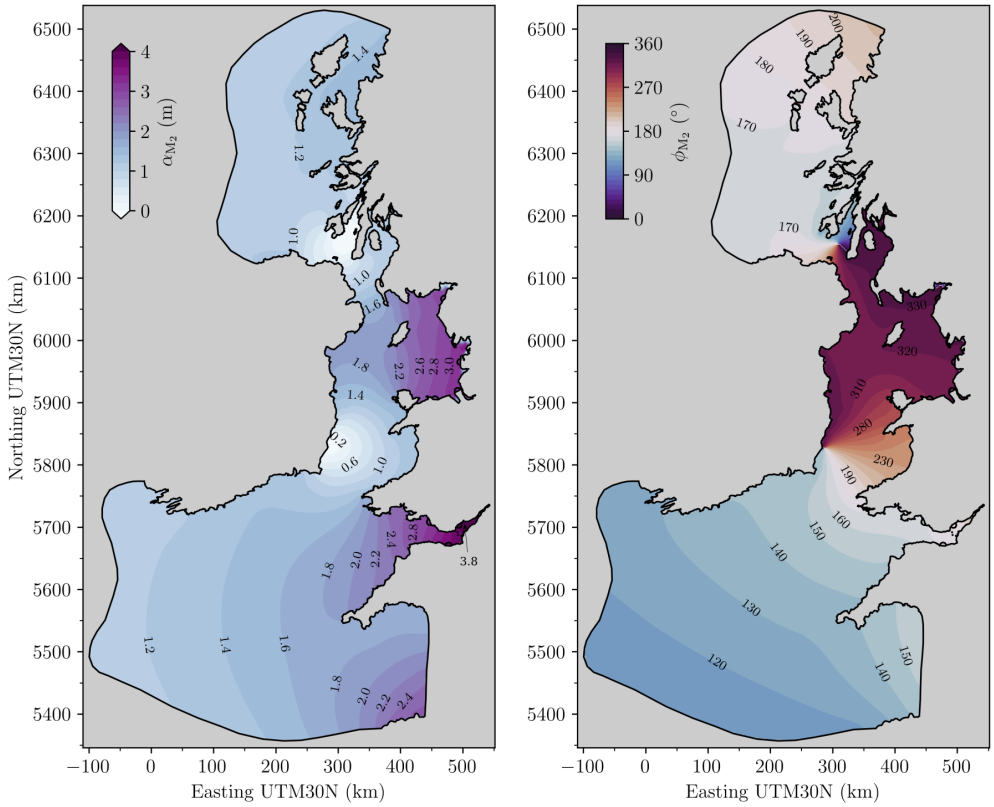

Figure 4: Principal tidal constituent M_2 amplitude α_{M_2} (m) and phase ϕ_{M_2} (°) across the ambient model domain, interpolated onto a 2 × 2 km grid for visualisation and diagnostic analysis purposes.

4.2. Impact on intertidal zones

The impact of tidal energy lagoons on the boundary between the open ocean and intertidal zones along the British coastline is investigated. Fig. 7 provides contours of the intertidal boundary (minimum total water depth $\min(D) = 0$ (m)) in four areas exhibiting a notable adjustment upon implementing regional tidal lagoons (i.e. BC lagoons or IS lagoons depending on the area) to the ambient model. While an intertidal boundary shift is apparent, changes are relatively small in comparison to the total breadth of the intertidal zone. Furthermore, there is little consistency as to whether the boundary shifts landwards or seawards, for the particular operational strategy imposed. Some deviations between model configurations may arise from slight differences in mesh discretisation. In Fig. 7, bathymetry h (m) is also displayed in order to illustrate areas that may potentially be sensitive to further intertidal boundary shifts as a result of changing tidal conditions. The inclusion of freshwater inflows in the model may also affect the location of the intertidal boundary.

The impact on the intertidal zones contained within the tidal lagoon impoundments is assessed temporally. Fig. 8 considers the changes induced within each tidal power plant impoundment perimeter by adding just the indicated tidal lagoon to the ambient model. In Fig. 8a, a time series of the transient dry zone surface

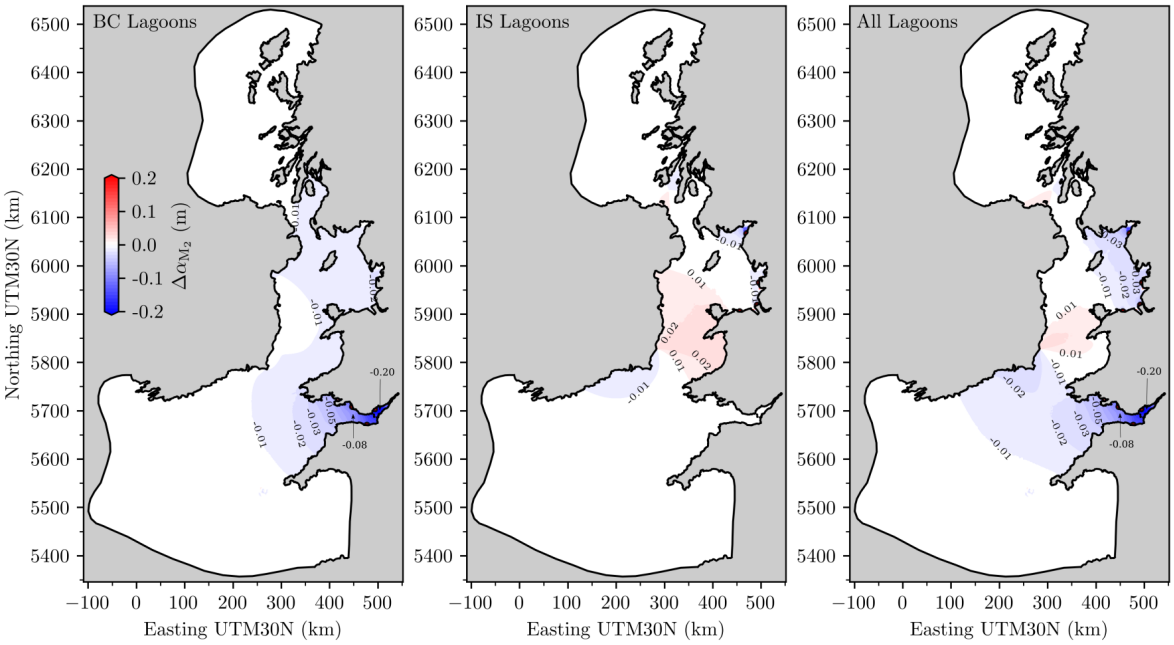

Figure 5: Changes in principal tidal constituent M_2 amplitude $\Delta\alpha_{M_2}$ (m) when applying tidal lagoons in the Bristol Channel only (BC), the Irish Sea only (IS) or in all considered locations to the ambient model. Results are interpolated onto a 2 × 2 km grid for visualisation and diagnostic analysis purposes.

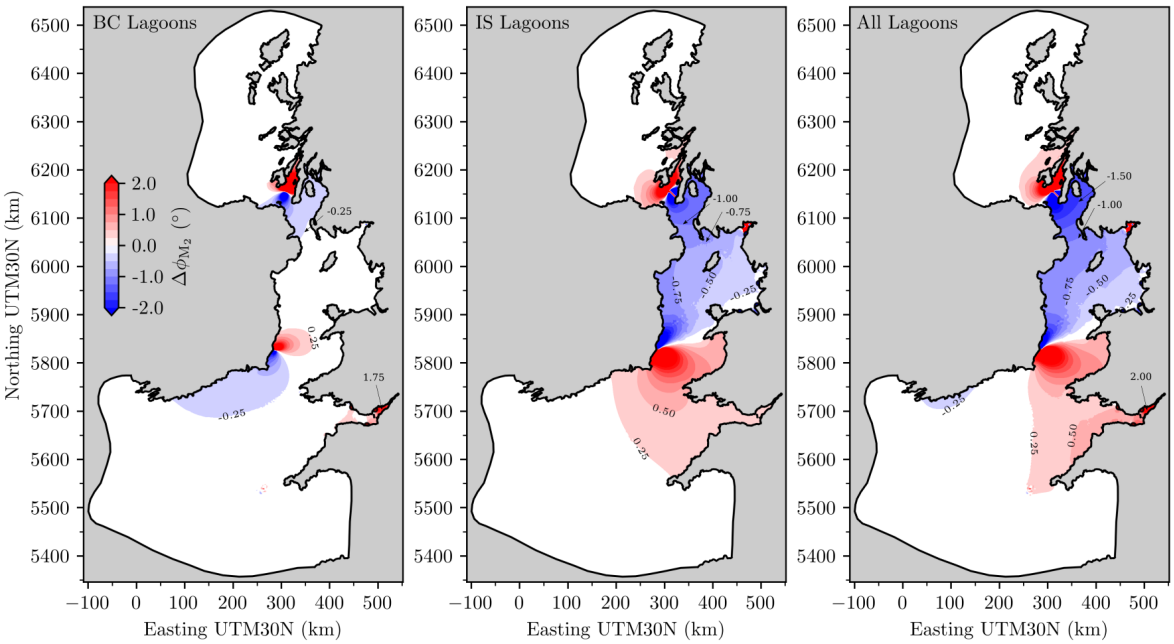

Figure 6: Changes in principal tidal constituent M_2 amplitude phase $\Delta\phi_{M_2}$ (°) when applying tidal lagoons in the Bristol Channel only (BC), the Irish Sea only (IS) or in all considered locations to the ambient model. Results are interpolated onto a 2 × 2 km grid for visualisation and diagnostic analysis purposes.

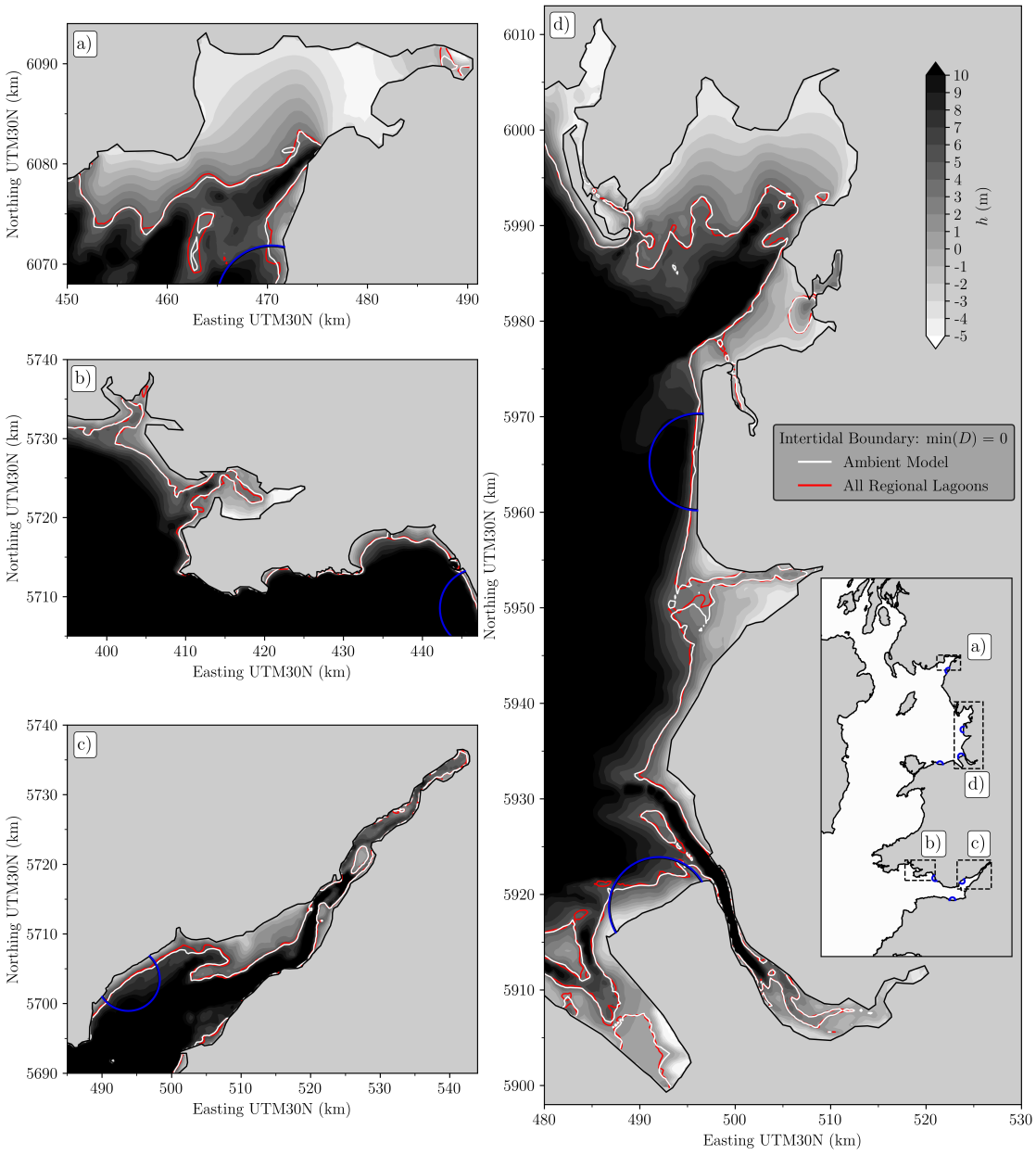

Figure 7: Bathymetry h (m) contour plot relative to mean water level (MWL) overlain with minimum total water depth min(D) = 0 (m) contours, indicating the boundary between the intertidal area and the ocean. Contours are provided for min(D) = 0 over the simulation period in both the ambient model (shown in white) and the model where all regional lagoons are included (BC or IS, shown in red). Indicated areas are a) Solway Firth, b) Carmarthen Bay and Swansea Bay, c) the Severn Estuary and d) a stretch of coastline along the north-west of England. Results are interpolated onto a 1 × 1 km grid for visualisation and diagnostic analysis purposes.

area A_{d} (km^2) is presented. The timing at which the intertidal zones dry is seen to consistently shift as a result of the tidal lagoon operating regimes. Meanwhile, A_{d} maximums increase in each impoundment area upon inclusion of each tidal lagoon, and remain at this maximum for a longer period of time. LI, BL and SO

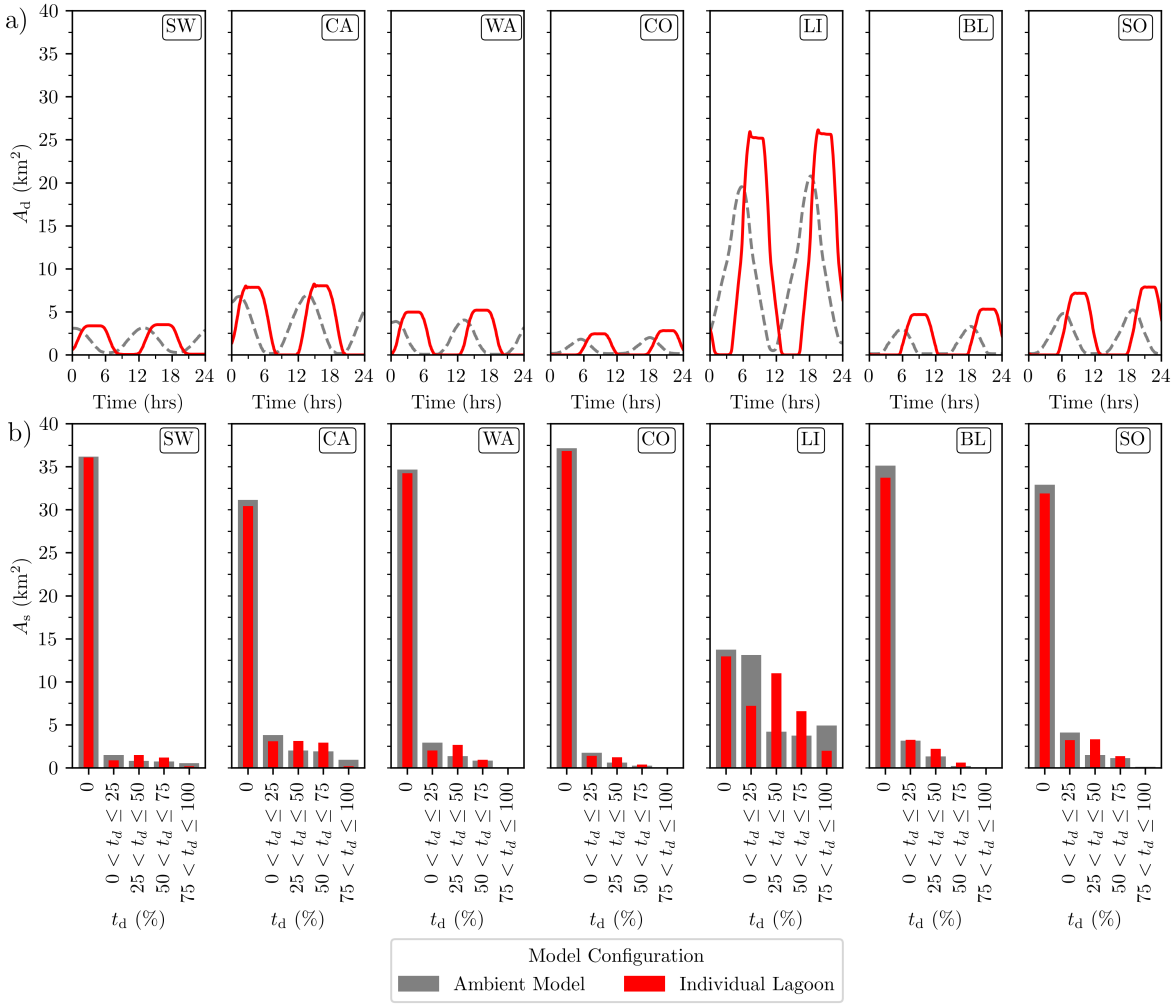

Figure 8: Time series comparing the intertidal areas within the tidal lagoon impoundment perimeters, in the ambient model and the models applying the indicated lagoon only. a) displays transient dry areas A_d (km^2), while b) indicates the surface area A_s (km^2) of the lagoon impoundments that are spent dry for the indicated percentages of time t_d.

experience the largest relative changes in A_d. Fig. 8b presents the change in impoundment surface area A_s that is spent dry for the indicated percentages of the simulation time t_d (%). The proportion of time that intertidal zones remain either wet or dry has a governing influence on both flora and fauna species habitat [70] and sediment type [71]. It can be observed that results generally combine an increase in A_s at $25\% < t_\mathrm{d} < 75\%$, with a decrease in A_s at $t_\mathrm{d} < 25\%$. As t_d is predominantly controlled by the operation regime implemented, this consistency can be attributed to the similar control periods applied on all the schemes (Table 4). However, the LI lagoon impoundment is here affected to the greatest degree.

4.3. Hydrodynamic impact

The hydrodynamic impact caused by siting and operating combinations of the seven tidal energy lagoons is assessed by investigating changes in the movement of water through transects. The locations of the nine transects are indicated on the map in Fig. 9. Seven of the transects span an area of water deemed likely to be affected by the presence and operation of their nearest tidal lagoon. The label assigned to the transect reflects this nearby tidal lagoon. A further two transects are situated at the threshold of each geographical region: at the mouth of the Bristol Channel (BC) and at a narrowing of the Irish Sea (IS) by Belfast.

Table 5: Comparing changes ($\Delta\%$) in length L_{T} (km), average cross sectional flow area $\overline{A_{\mathrm{T}}}$ (m^2) and mean flux peaks $\overline{Q_{\mathrm{T,p}}}$ and troughs $\overline{Q_{\mathrm{T,t}}}$ ($\mathrm{m}^3\mathrm{s}^{-1}$) across nine transects when implementing either their nearby 'individual' tidal lagoon (of the same label) or all 'regional' lagoons (BC or IS tidal lagoons) to the 'ambient' model. $\Delta\% < 0$ indicates that the associated metric is adjusted closer to 0, including $\overline{Q_{\mathrm{T,t}}}$. Positive flux, is defined as having a seawards trajectory i.e. outflows (perpendicular to the transects in the directions indicated on Fig. 9).

Transect	**Model**	L_{T} (km)	$\overline{A_{\mathrm{T}}}$ (m^2)	$\overline{Q_{\mathrm{T,p}}}$ ($\mathrm{m}^3\mathrm{s}^{-1}$ $\times 10^3$)	$\overline{Q_{\mathrm{T,t}}}$ ($\mathrm{m}^3\mathrm{s}^{-1}$ $\times 10^3$)
BC	Ambient	69.6	3,231,075	2,137	−2,277
	Regional ($\Delta\%$)	-	-	−5.6%	−2.7%
SW	Ambient	34.7	829,686	845	−871
	Individual ($\Delta\%$)	−21.0%	−9.2%	−1.6%	−1.2%
	Regional ($\Delta\%$)	−21.0%	−9.2%	−8.7%	−3.8%
WA	Ambient	21.7	408,636	479	−501
	Individual ($\Delta\%$)	−23.3%	−18.0%	−4.6%	−3.2%
	Regional ($\Delta\%$)	−23.3%	−18.0%	−10.2%	−5.1%
CA	Ambient	14.0	160,488	174	−186
	Individual ($\Delta\%$)	−36.4%	−17.7%	−3.1%	−1.9%
	Regional ($\Delta\%$)	−36.4%	−17.7%	−4.5%	−1.4%
IS	Ambient	37.0	3,745,446	3,216	−3,259
	Regional ($\Delta\%$)	-	-	−0.4%	+0.0%
SO	Ambient	22.7	123,765	79	−99
	Individual ($\Delta\%$)	−24.4%	−36.4%	−9.5%	−6.9%
	Regional ($\Delta\%$)	−24.4%	−36.4%	−8.1%	−6.7%
BL	Ambient	20.2	140,564	121	−133
	Individual ($\Delta\%$)	-	+4.3%	+0.6%	+0.2%
	Regional ($\Delta\%$)	-	+4.3%	+0.0%	+1.6%
LI	Ambient	1.9	20,537	26	−27
	Individual ($\Delta\%$)	-	+1.7%	−0.3%	−0.1%
	Regional ($\Delta\%$)	-	+1.7%	+0.3%	+0.1%
CO	Ambient	164.0	5,813,102	2,494	−2,999
	Individual ($\Delta\%$)	−3.1%	−1.3%	−0.7%	−0.5%
	Regional ($\Delta\%$)	−3.1%	−1.3%	−2.2%	−1.5%

Certain transects intersect the embankment of their corresponding scheme in configurations of the model including tidal lagoons. These are therefore truncated from the transects in the ambient model so as to not

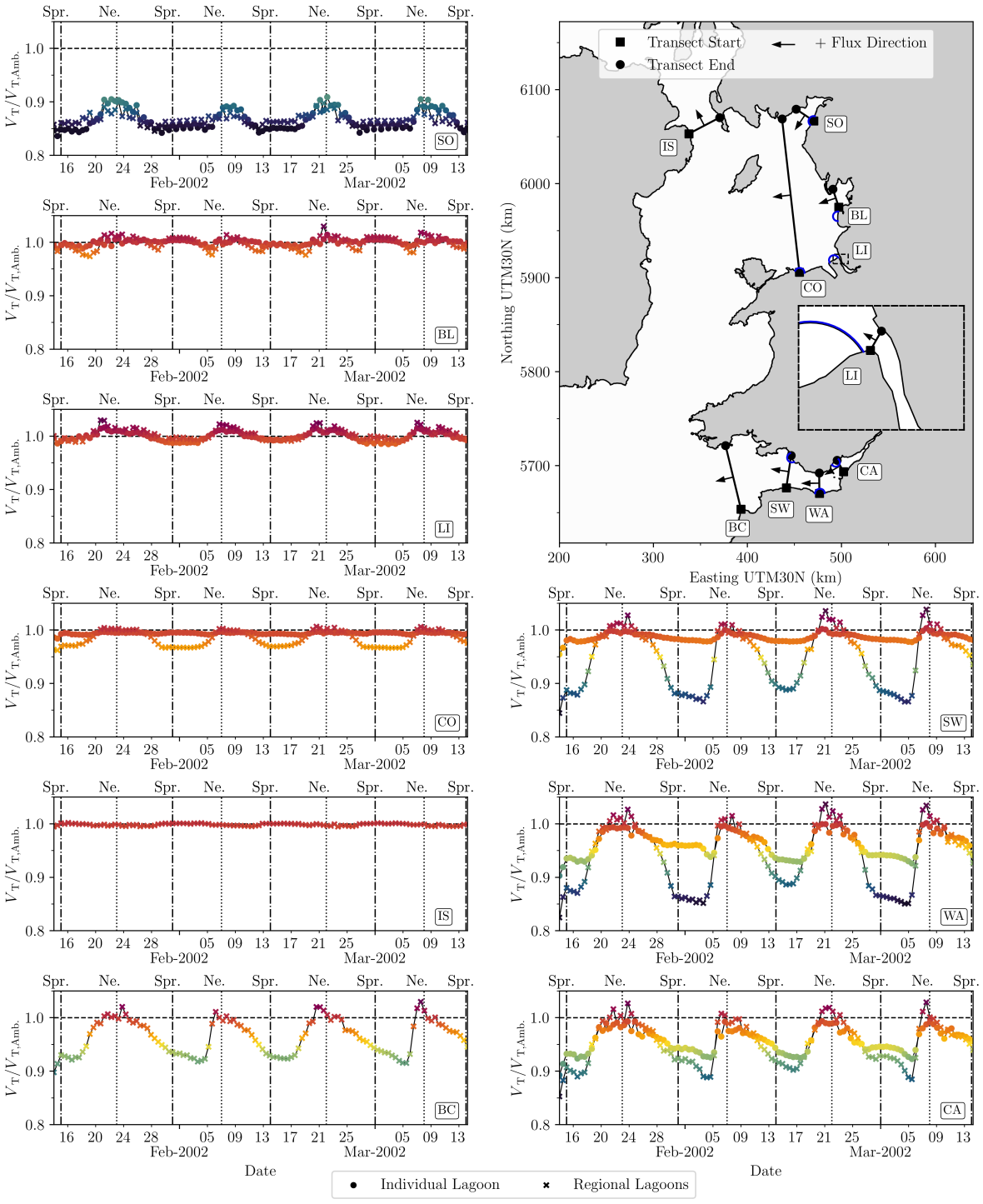

Figure 9: Time series of total volume exchange per tidal cycle V_T (m^3) of the numerical model including tidal lagoons, normalised against the ambient model $V_{T,Amb.}$. 'Individual lagoon' refers to the model configuration containing just the nearest lagoon to the transect with the same corresponding label as in Fig. 2. 'Regional lagoons' refers to the model configuration containing all the tidal lagoons in the associated region (Bristol Channel or Irish Sea). Occurrences of spring (Spr.) and Neap (Ne.) tides are also indicated.

include the impoundment area. Table 5 provides resulting alterations ($\Delta\%$) in both the length L_{T} (km) and average cross sectional flow area $\overline{A_{\mathrm{T}}}$ (m^2) of the transect when applying the indicated tidal lagoons. The LI and BL transects do not intersect with their corresponding tidal lagoon, but their $\overline{A_{\mathrm{T}}}$ is marginally increased upon addition of the schemes due to a resulting change in the mesh configuration. Of the truncated transects, only SO experiences a larger decrease in $\overline{A_{\mathrm{T}}}$ than L_{T}. This is a result of the SO tidal lagoon being situated in the deeper section of the transect. Meanwhile, the SW, WA and CA tidal lagoons cross the shallower end of the transects.

Table 5 characterises hydrodynamics through the transects by computing a time series of flux Q_{T} ($\mathrm{m}^3\mathrm{s}^{-1}$), extracting peaks ($Q_{\mathrm{T,p}}$) and troughs ($Q_{\mathrm{T,t}}$) and calculating their respective means ($\overline{Q_{\mathrm{T,p}}}$ and $\overline{Q_{\mathrm{T,t}}}$). The direction of positive flux (and in turn $\overline{Q_{\mathrm{T,p}}}$) has been defined as outflows (i.e. exiting the channel or bay). Results are provided for the ambient model, while the impacts of implementing individual nearby lagoons (where applicable) or all the tidal lagoons in the same region are quantified as a percentage difference ($\Delta\%$) from ambient conditions. Total volume exchange per tidal cycle V_{T} (m^3) is calculated via methodology outlined in Section 2.4 and plotted as a time series in Fig. 9. Time dependent V_{T} values for models applying individual tidal lagoons and all regional lagoons are normalised against V_{T} in the ambient model $V_{\mathrm{T,Amb.}}$: $V_{\mathrm{T}}/V_{\mathrm{T,Amb.}}$.

In Table 5, ambient model inflows in the Bristol Channel decrease landwards through the transects (rising $\overline{Q_{\mathrm{T,t}}}$ from BC to CA), whilst outflows increase seawards (rising $\overline{Q_{\mathrm{T,p}}}$ from CA to BC). Here, implementing tidal lagoons individually is shown to decrease flux through associated transects. The greatest impact on $\overline{Q_{\mathrm{T,p}}}$ and $\overline{Q_{\mathrm{T,t}}}$ is observed at the WA transect. The addition of all regional Bristol Channel tidal lagoons impact hydrodynamics further, a trend also apparent in Fig. 9. In the Irish Sea, configurations of the model with individual tidal lagoons affect ambient hydrodynamics in the nearby transects ($\Delta\%$) to a relatively small degree. A notable exception is the SO transect. When all regional tidal lagoons are applied, few further impacts are present, apart from at CO which spans the whole region.

Some trends can be observed in all considered transects. Greater absolute values of ambient $\overline{Q_{\mathrm{T,t}}}$ than $\overline{Q_{\mathrm{T,p}}}$ are present, suggesting that inflows are more dynamic than outflows. However, Table 5 indicates that outflows ($\overline{Q_{\mathrm{T,p}}}$) are consistently more impacted than inflows ($\overline{Q_{\mathrm{T,t}}}$) by individual and regional implementation of tidal lagoons. Furthermore, Fig. 9 illustrates how the more energetic spring tide dynamics are impacted to a greater degree than the neap tide dynamics.

4.4. Impact on stratification

The Simpson Hunter Index (SHI) [41] is applied as a method for locating mixing fronts. SHI $< 2.7 \pm 0.3$ $\mathrm{m}^{-2}\mathrm{s}^3$ suggests well-mixed conditions, whereas SHI $> 2.7 \pm 0.3$ $\mathrm{m}^{-2}\mathrm{s}^3$ suggests stratified flow. Mean SHI over the simulation period, $\overline{\mathrm{SHI}}$, is considered here. Section 4.4a indicates $\overline{\mathrm{SHI}}$ in the ambient model, with contours

highlighting mixing fronts. Section 4.4b shows how ambient fronts are affected upon the implementation of all seven tidal power lagoons. The ambient model experiences stratified flow in the majority of the domain, with well-mixed conditions occurring typically in channels, inlets and around headlands. Alterations to the mixing fronts upon addition of the tidal power lagoons are minor, with the most notable changes taking place
365 at the mouth of the Bristol Channel. Here, areas susceptible to stratified flow are shown to shift further into the channel. A 3D model would provide greater insight into the dynamics of stratified flows, but the 2D approach applied here is sufficient for the aims of this study as resonant areas containing tidal lagoons are generally well-mixed.

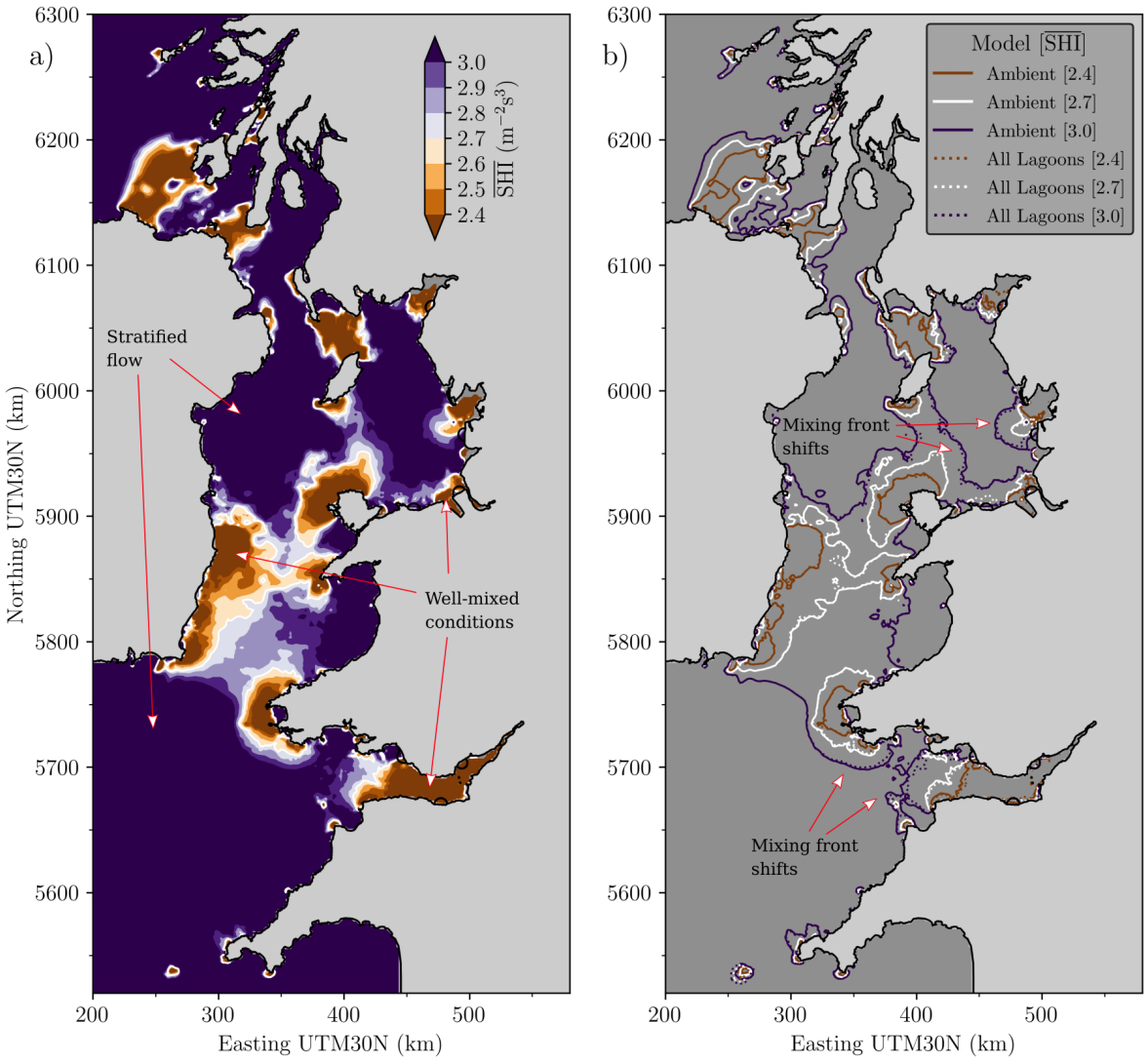

Figure 10: Contour plots displaying $\overline{\text{SHI}}$ (average Simpson Hunter Index, m^{-2}s^3). The critical value range of $\overline{\text{SHI}} = 2.7 \pm 0.3$ m^{-2}s^3 is highlighted. a) illustrates ambient conditions. b) presents changes induced by applying all considered tidal lagoons. Results are interpolated onto a 2 × 2 km grid for visualisation and diagnostic analysis purposes.

4.5. Impact on bed shear stress

The impact of the tidal energy lagoons on morphology is here investigated by quantifying changes Δ to ambient mean bed shear stress magnitude $\overline{|\tau_b|}$: $\Delta\overline{|\tau_b|}$ (both kgm^{-1}s^{-2}). Fig. 11 and Fig. 12 highlight $\overline{|\tau_b|}$ in the ambient model, and $\Delta\overline{|\tau_b|}$ when considering the indicated tidal energy lagoons in solely the Bristol Channel (BC) and Irish Sea (IS), respectively.

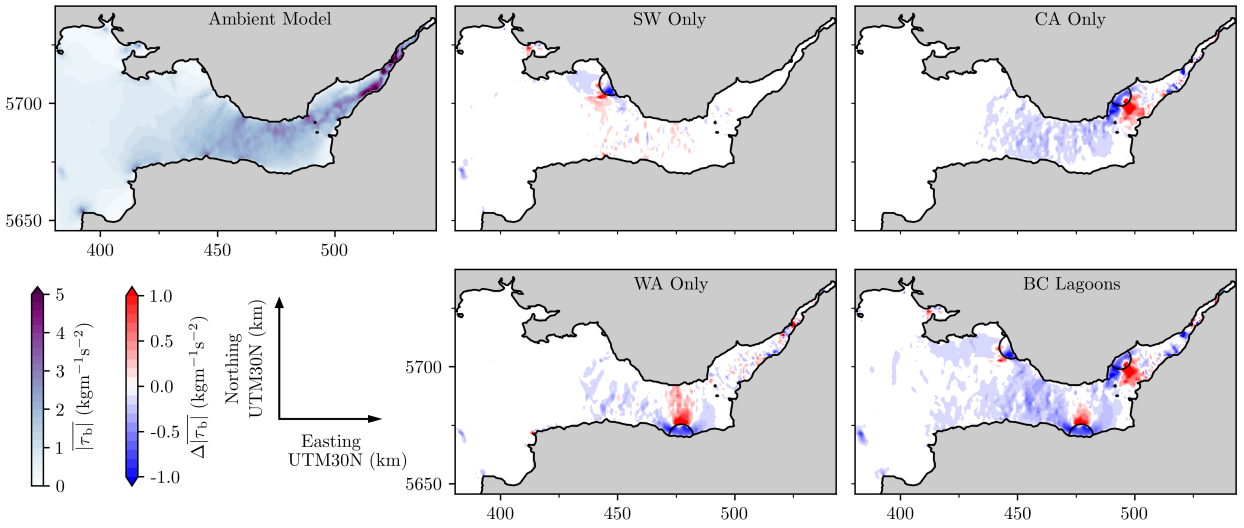

Figure 11: Ambient mean bed shear stress magnitude $\overline{|\tau_b|}$ (kgm^{-1}s^{-2}) in the Bristol Channel region and the resulting changes $\Delta\overline{|\tau_b|}$ when implementing indicated combination of tidal lagoons. Results are interpolated onto a 1 $\times$ 1 km grid for visualisation and diagnostic analysis purposes.

The Bristol Channel (Fig. 11) is a highly dynamic region, as reflected by large areas of high $\overline{|\tau_b|}$ in the ambient model. High increases ($\Delta\overline{|\tau_b|} \gg 0$ kgm^{-1}s^{-2}) exist in the path of hydraulic structure outflows in all configurations of the model. Elsewhere in the Bristol Channel, large areas of $\Delta\overline{|\tau_b|} < 0$ kgm^{-1}s^{-2} are present. SW can be seen to have a lesser overall effect on changes in $\overline{|\tau_b|}$ than CA and WA. When all three tidal energy lagoons are applied (BC Lagoons), their cumulative effect on $\Delta\overline{|\tau_b|}$ noticeably spans the whole Bristol Channel. In this regional model, some areas experience little net change in $\overline{|\tau_b|}$ due to a combination of increases and decreases induced by the different tidal energy lagoons.

In Fig. 12, an overall lower ambient mean bed shear stress magnitude $\overline{|\tau_b|}$ is observed in the Irish Sea compared the Bristol Channel (Fig. 11). Upon applying tidal lagoons in the Irish Sea (IS Lagoons), $\Delta\overline{|\tau_b|} > 0$ kgm^{-1}s^{-2} is present at hydraulic structure outflows, consistently with tidal energy lagoons added in the Bristol Channel. In both Fig. 11 and Fig. 12, a pattern emerges in that a higher impact on $\overline{|\tau_b|}$ at these outflows occurs where a higher reduction in average cross sectional flow area $\overline{A_T}$ (m^2) is present (Table 5), specifically WA, CA and SO. Aside from turbine and sluice outflows, noticeable changes in $\overline{|\tau_b|}$ are generally

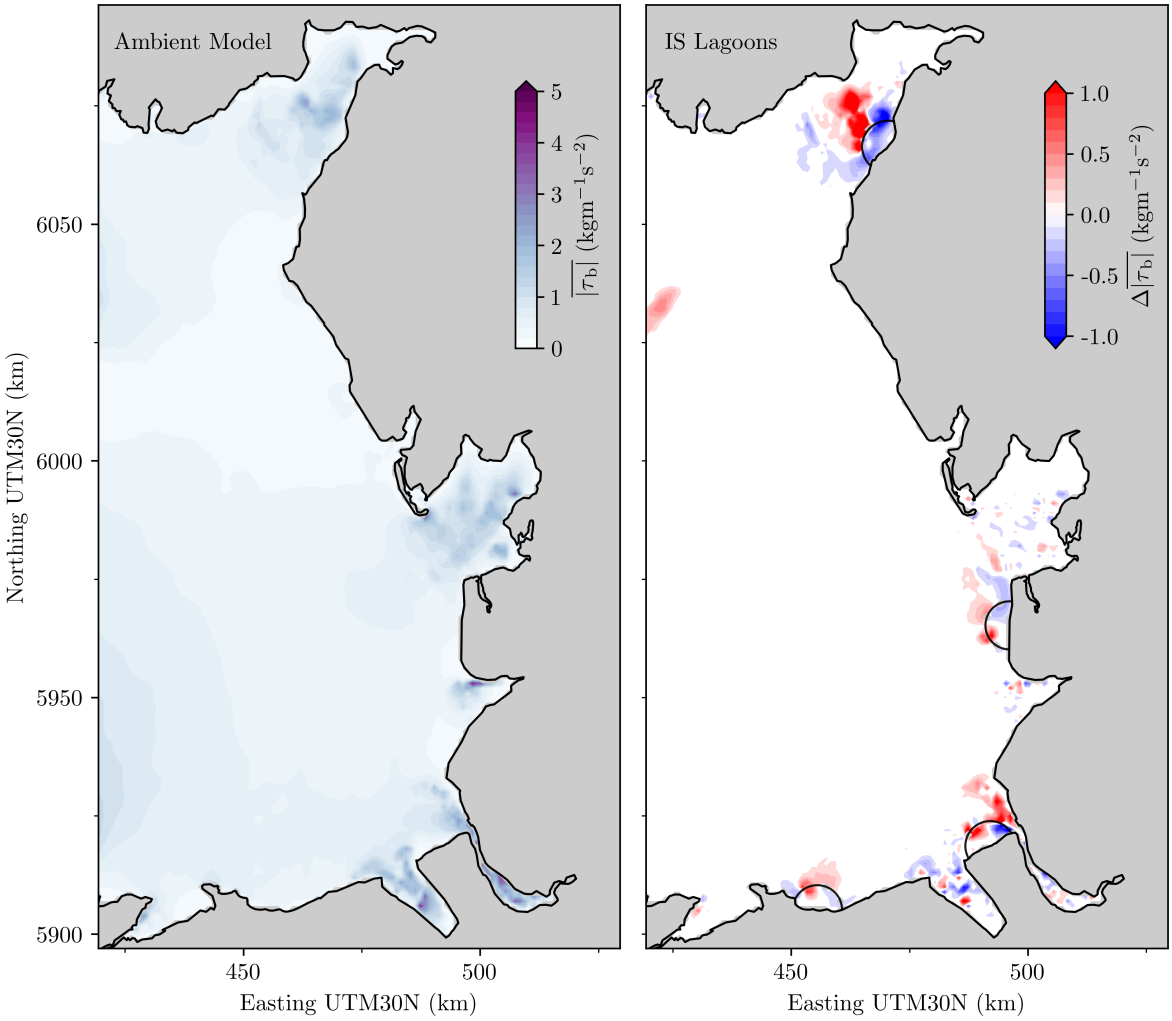

Figure 12: Ambient mean bed shear stress magnitude $\overline{|\tau_b|}$ (kgm^{-1}s^{-2}) in the Irish Sea region and the resulting changes $\Delta\overline{|\tau_b|}$ when implementing indicated combination of tidal lagoons. Results are interpolated onto a 1 × 1 km grid for visualisation and diagnostic analysis purposes.

limited to nearby inlets. A notable exception is the entrance to the Mersey river, which is severely narrowed by the presence of the LI tidal lagoon and thus experiences a large increase in $\overline{|\tau_b|}$. Section D in the Supplementary Material provides $\Delta\overline{|\tau_b|}$ when individual tidal power lagoons are applied in the Irish Sea region.

4.6. Energy resource impact

Impacts on the tidal energy resource are investigated using two methods. Firstly, impact (Δ) on ambient theoretical annual available energy $E_{A,yr}$ (GWh km^{-2}) is quantified spatially at a regional scale. Secondly, changes that arise between estimated annual energy output E_{yr} (GWh) of individual and multiple tidal energy lagoons is calculated. Details of both methodologies are outlined in Section 2.4.

Fig. 13 displays $E_{\mathrm{A,yr}}$ of the ambient model in the Bristol Channel. The other sub-figures show the impact on $E_{\mathrm{A,yr}}$ ($\Delta E_{\mathrm{A,yr}}$) when implementing the labelled tidal power lagoons to the ambient model. Outside of the tidal lagoon impoundments (where $E_{\mathrm{A,yr}}$ increases due to pumping intervals), $\Delta E_{\mathrm{A,yr}} < 0$ GWh km^{-2} is exhibited throughout the region. It can be seen that the spatial extent of affected areas is roughly similar upon the addition of each individual tidal lagoon, spanning the majority of the Bristol Channel. The magnitude of the decrease in $E_{\mathrm{A,yr}}$ is consistently higher towards the river mouth to the east coast. The closer the power plant is situated to the river mouth, the higher its overall impact. The CA lagoon affects the energy resource of the Bristol Channel to the greatest degree, whilst also suffering the greatest loss in $E_{\mathrm{A,yr}}$ upon addition of all tidal lagoons in the channel. This is the case for both $\Delta E_{\mathrm{A,yr}}$ in absolute terms (as displayed) and relative terms, despite the higher ambient resource in the upper Severn Estuary.

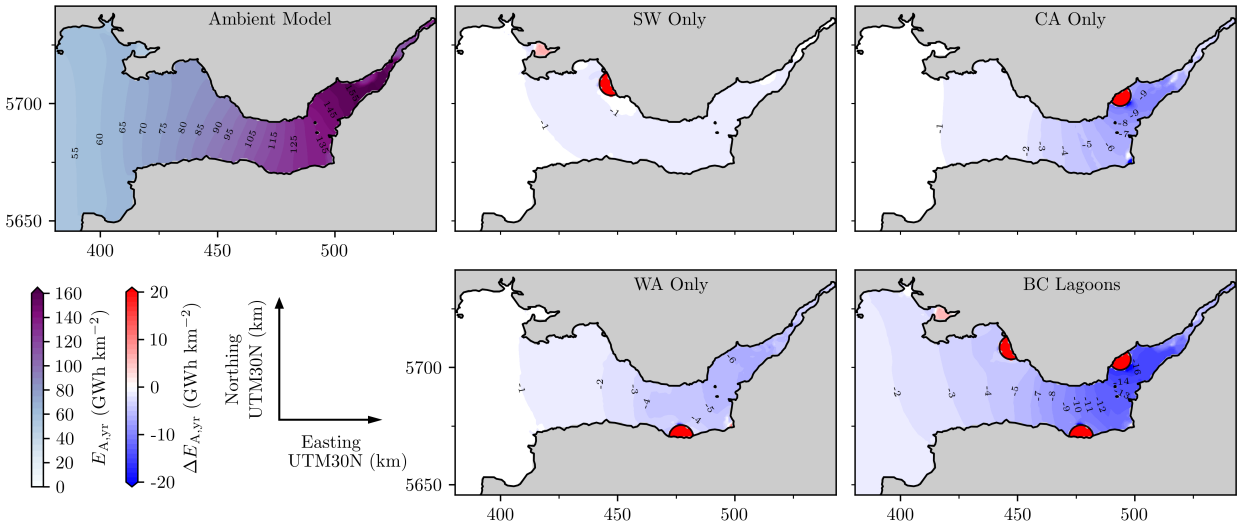

Figure 13: Ambient annual theoretical energy resource $E_{\mathrm{A,yr}}$ (GWh km^{-2}) in the Bristol Channel region and the resulting changes $\Delta E_{\mathrm{A,yr}}$ when implementing indicated combination of tidal lagoons. Results are interpolated onto a 1 × 1 km grid for visualisation and diagnostic analysis purposes.

In Fig. 14, ambient $E_{\mathrm{A,yr}}$ is shown for the Irish Sea region. Impacts in the wider region are negligible, and each individual tidal lagoon imposes little impact on the energy resource of the other power plants in the region. Therefore, $\Delta E_{\mathrm{A,yr}}$ is only provided for the configuration with all tidal power lagoons in the Irish Sea. The most notable decreases in $E_{\mathrm{A,yr}}$ occur in the Solway Firth (nearby the SO lagoon) and Morecambe Bay (by the BL lagoon), as well as other inlets. Section D in the Supplementary Material illustrates $\Delta E_{\mathrm{A,yr}}$ in cases where when individual tidal power lagoons in the Irish Sea region are implemented.

Table 6 presents the proportion of $\overline{E_{\mathrm{A,yr}}}$ (the mean of $E_{\mathrm{A,yr}}$ within the lagoon impoundments) converted by each tidal power lagoon when applied to the 2D model individually. CA and WA tidal lagoons are shown to

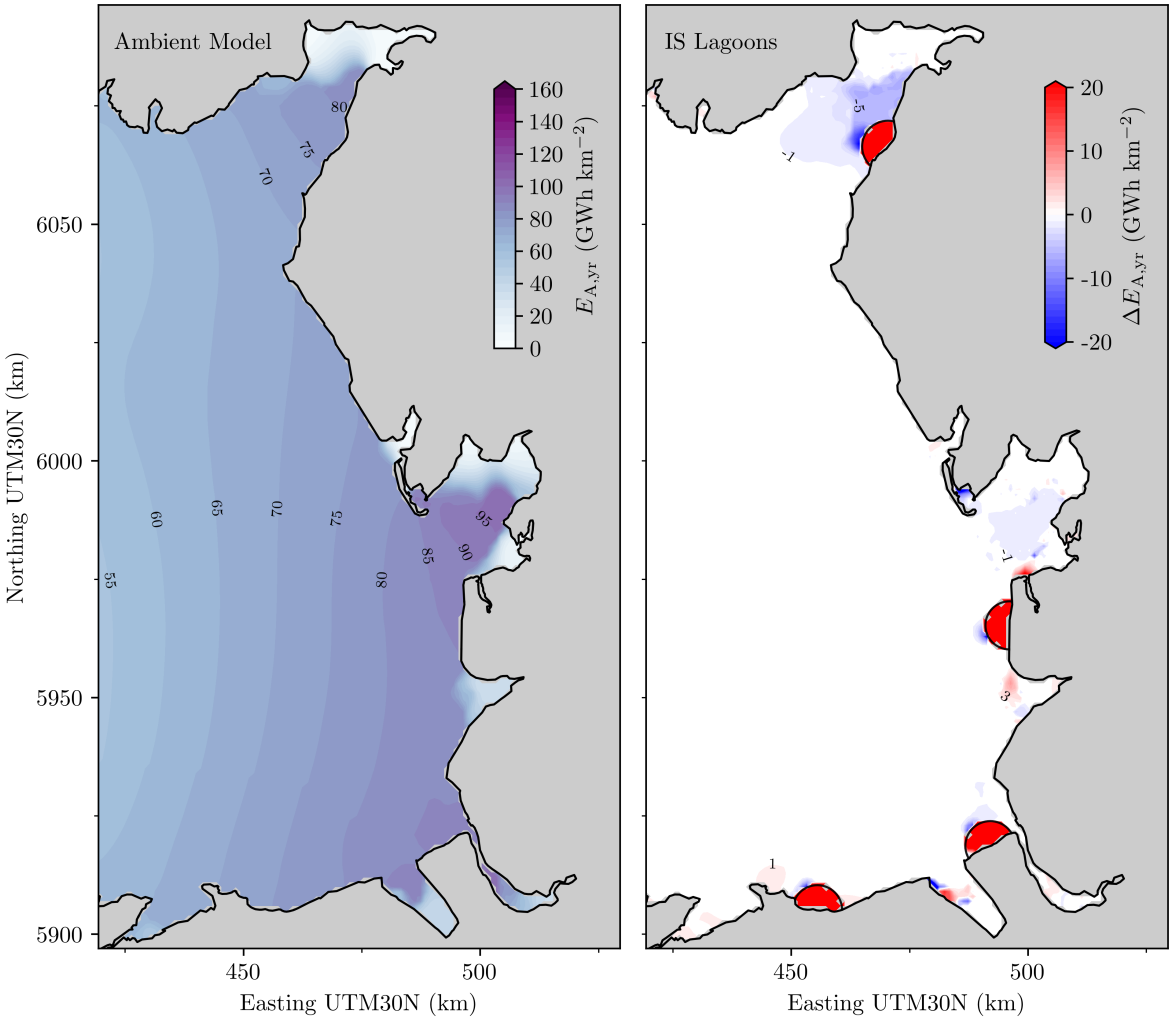

Figure 14: Ambient annual theoretical energy resource $E_{\mathrm{A,yr}}$ (GWh km^{-2}) in the Irish Sea region and the resulting changes $\Delta E_{\mathrm{A,yr}}$ when implementing indicated combination of tidal lagoons. Results are interpolated onto a 1×1 km grid for visualisation and diagnostic analysis purposes.

contain the most energetic resource $\overline{E_{\mathrm{A,yr}}}$, but also have among the lowest extraction rates. Of the remaining tidal lagoons, LI has the highest $\overline{E_{\mathrm{A,yr}}}$, yet generates the lowest annual energy output E_{yr}.

In Table 7, annual tidal lagoon energy output E_{yr} (GWh) is quantified as a percentage change ΔE_{yr} between the model including tidal lagoons individually (quantities are provided in Table 6), and the model including the indicated combination of tidal lagoons. It is evident that certain tidal lagoon construction locations are more susceptible to a reduction in E_{yr} than others. The largest impact can be observed at the CA tidal lagoon, which experiences $\Delta E_{\mathrm{yr}} \approx -11\%$ when the other lagoons in the Bristol Channel are operating. A smaller reduction is predicted for SW, with all other candidate locations experiencing $\Delta E_{\mathrm{yr}} > -2\%$ when regional tidal lagoons are present. CO even generates with a higher energy output. There is also a small, but notable difference between the ΔE_{yr} when including only regional tidal lagoons, and when

operating all seven tidal lagoons.

Table 6: An estimation of the proportion of annual theoretical energy resource $\overline{E_{\mathrm{A,yr}}}$ (GWh km^{-2}) converted by each tidal power lagoon when applied individually to the 2D model, via $E_{\mathrm{yr}}/(\overline{E_{\mathrm{A,yr}}}\ \overline{A_{\mathrm{w}}})$, where E_{yr} (GWh) is the annual energy output predicted by the 2D model and $\overline{A_{\mathrm{w}}}$ the mean wetted surface area of the impoundment (km^2). Site-specific values of $\overline{A_{\mathrm{w}}}$ are provided in Table 4.

2D Model: / **Scheme:**	**Ambient** $\overline{E_{\mathrm{A,yr}}}$ (GWh km^{-2})	**Individual Lagoon** E_{yr} (GWh)	**Extraction Rate** $E_{\mathrm{yr}}/(\overline{E_{\mathrm{A,yr}}}\ \overline{A_{\mathrm{w}}})$ (%)
SW	81	1,803	58.1%
CA	146	2,538	47.4%
WA	121	2,527	54.0%
CO	75	1,679	57.1%
LI	86	1,388	52.7%
BL	85	1,824	54.7%
SO	78	1,644	55.4%
BC Lagoons Total	-	6,868*	52.3%
IS Lagoons Total	-	6,535*	55.0%
All Lagoons Total	-	13,403*	53.6%

* Combined totals of E_{yr} for individual lagoon model configurations serve solely a comparative purpose.

Table 7: Difference in annual energy output E_{yr} (GWh/year), ΔE_{yr} (%), between model configurations implementing individual tidal lagoons (E_{yr} provided in Table 6) and the indicated power plant combinations.

2D Model: / **Scheme:**	**All Lagoons** ΔE_{yr} (%)	**BC Lagoons** ΔE_{yr} (%)	**IS Lagoons** ΔE_{yr} (%)
SW	−5.9%	−5.6%	-
CA	−9.1%	−11.3%	-
WA	−0.9%	−1.3%	-
CO	−1.1%	-	+3.2%
LI	−1.1%	-	+0.8%
BL	−1.2%	-	−1.2%
SO	−3.3%	-	−1.9%
BC Lagoons Total	−5.3%	−6.1%	-
IS Lagoons Total	−1.6%	-	+0.2%
All Lagoons Total	−3.5%	-	-

5. Discussion

Both regional and localised aspects of the marine environment influence tidal energy lagoon impacts along the west coast of Great Britain. The two distinct but tidally connected geographical regions in this study exhibit contrasting characteristics. The Bristol Channel contains estuarine coastal geometry which narrows landwards and facilitates a resonant tidal wave with a relatively straight trajectory. The Irish Sea, meanwhile,

is a much larger body of water with less constrained geometry, but contains an extensive distribution of bays and inlets. Certain results presented in this paper can be compared directly with other numerical modelling studies which focus on impacts of tidal power developments in these two regions [5, 6, 16, 18, 23, 24, 25, 28]. Discrepancies with the literature could potentially arise from a) modelling configuration decisions, b) differences between the impacts of tidal lagoons and tidal barrages, c) inconsistencies in tidal lagoon design or d) operation strategies; these are discussed below where appropriate.

5.1. Influence of regional geometry

A key consequence of regional geometry is the extent to which individual tidal lagoons physically impede macro-tidal processes. Tidal barrages in river estuaries, for example, generate 100% blockage by definition, and their impact on tidal resonance has been discussed in relation to the Severn Barrage [5, 72, 73]. It can be seen in Fig. 2 how the tidal power lagoons in the Bristol Channel (SW, CA and WA) typically lie closer to the coast opposite to which they are situated than those in the Irish Sea (CO, LI and BL). An exception to this pattern is the SO lagoon. However, SO blockage is more localised, and the embankment doesn't protrude significantly into the main body of the region.

The greater degree of tidal lagoon blockage present in the Bristol Channel appears to noticeably dampen resonance effects. In Fig. 5, one can observe that BC Lagoons trigger alterations in principal tidal constituent M_2 amplitude of $-0.02 > \Delta\alpha_{\mathrm{M}_2} > -0.20$ m throughout the region, with minor far-field decreases also detected across the Irish Sea. Meanwhile, IS lagoons have a lesser impact on regional tidal resonance owing to their lower blockage. Negligible $\Delta\alpha_{\mathrm{M}_2}$ is detected in the main body of the region north of Wales. These observations can also be in part attributed to the natural period of the Bristol Channel being closer to quarter wave-length resonance than the Irish Sea [72], and is thus more susceptible to changes in amplitude when this is disturbed. In addition, the most prominent change in mixing fronts occur at the threshold of the Bristol Channel(Fig. 10), a result of the greater degree of tidal lagoon blockage in this region.

Wolf et al. [24] and Yates et al. [25] report similar $\Delta\alpha_{\mathrm{M}_2}$ trends, albeit significantly magnified in the upper reaches of the Severn Estuary and at inlets in the Irish Sea (e.g. Morecambe Bay and Solway Firth). The location of ambient mixing fronts reported here reflect findings in the work of Wolf et al. [24], but locational shifts resulting from tidal power developments are here less pronounced. By contrast, Zhou et al. [18] and Angeloudis and Falconer [28] predict an increase in maximum water levels ($\Delta\alpha_{\mathrm{M}_2}$ is connected) downstream of the Severn Barrage in the Bristol Channel. In addition, a larger impact in water levels surrounding tidal lagoon developments nearby the LI and CO schemes is presented in Angeloudis et al. [6]. Magnifications [24, 25] and opposing effects [18, 28] stem from the the application of tidal barrages in these studies, and the increased blockage they induce. Further discrepancies may arise from differences in adopted operational strategies, but likely to a greater degree from the location at which the boundary forcing is imposed [6, 28].

The importance of open boundary location in assessing tidal lagoon impacts has been demonstrated in Section 3.3.1. Future tidal lagoon assessment studies may need to locate the open ocean boundaries at the continental shelf to fully capture changes in resonance, as has been reported for tidal barrages [5, 18, 62].

5.2. Linearity of cumulative regional impacts

It is suggested in Section 4.1 that impacts of tidal energy developments (namely, changes in M_2 amplitude $\Delta\alpha_{\mathrm{M}_2}$ (m)) in the Bristol Channel and Irish Sea combine linearly. Impacts arising from each specific region will not be magnified or reduced by impacts arising from the other region, but instead added to them. This relationship between the two regions has been discussed previously by Yates et al. [25]. However, it was found there that summing predicted $\Delta\alpha_{\mathrm{M}_2}$ of individual scheme developments resulted in much more magnified $\Delta\alpha_{\mathrm{M}_2}$ than predicted by the model with all considered schemes, indicating notable non-linearity [25]. This contrast in results suggests that impacts resulting from tidal range developments in the Bristol Channel and Irish Sea are therefore not inherently linear, but instead, that non-linear effects are near negligible in the lagoon-based case study applied here. The study by Yates et al. [25] applied tidal barrages in both regions, so the higher blockage could potentially magnify non-linearities. As tidal range developments have been frequently proposed in both regions (Table 1), future studies exploring tidal power plant combinations should acknowledge potential regional non-linearities, and consider the need for assessing candidate schemes in the same model. Here, non-linear effects are minimal in the employed numerical model, due to the more modest scale of developments considered. The nature of more localised impacts arising from tidal power lagoons in the two distinct regions can therefore be investigated separately.

5.3. Influence of the local marine environment

Localised marine environment characteristics are shown to greatly influence the impact of tidal lagoons on hydrodynamic metrics (Table 5 and Fig. 9). The transects in the Bristol Channel region are roughly parallel, with each spanning the y-axis of the main channel (BC, SW, WA and CA from west to east), and thus capturing the evolution of hydrodynamics. When modelled individually, WA and CA yield a notable decrease in flow compared to ambient conditions, to a greater degree than SW. This is a result of the manner in which they induce a higher degree of blockage in the Bristol Channel, and therefore act as choke points restricting flow locally. SW, meanwhile, protrudes less into the main channel.

The relationship between the SW and CA (but not WA) locations is explored in the study of Angeloudis and Falconer [28]. Large scale tidal lagoons in the CA location are shown to cause only slight changes in maximum velocity magnitude in the SW location (where a smaller-scale tidal lagoon is proposed, the 'Swansea Bay tidal lagoon') [28]. Similarly, Fig. 11 of this study demonstrates how SW and CA trigger little change in mean bed shear stress magnitude $\Delta\overline{|\tau_{\mathrm{b}}|}$ (an indicator of changes in velocity magnitude) at the other location.

Section 4.3 reports fewer cumulative impacts from simultaneous implementation of the Irish Sea tidal lagoons (CO, LI, BL and SO) than from the Bristol Channel tidal lagoons (SW, CA, WA). While this can in part be attributed to the Irish sea being larger than the Bristol Channel, Fig. 2 illustrates how the distance between CO, LI and BL is comparable to the lagoons in the Bristol Channel. The modelled localisation of impacts is instead facilitated to a greater degree by the less constrained geometry of the Irish Sea (Section 5.1). Impacts predominantly surround the structures themselves, and nearby inlets or bays. An increase in mean bed shear stress magnitude $\Delta\overline{|\tau_b|}$ ($\mathrm{kgm^{-1}s^{-2}}$) at hydraulic structure outflows is reported in both regions, in locations where tidal lagoons are situated nearby an opposing coastline. If economically feasible, a redistribution of turbines and sluices to sections of the embankment not immediately opposite a coastline could mitigate this. In Fig. 12, LI effectively shifts the mouth of the Mersey river estuary, thereby triggering a high increase in $\Delta\overline{|\tau_b|}$ along with a reduction in the Liverpool Bay. While this effect is observed at LI in the literature [6], the consistent tidal lagoon design in this study allows a direct contrast with tidal lagoons in other locations. BL and CO do not directly impede the in- or outflows of a resonant bay or inlet, and thus impacts are less evident. SO impedes flux into the Solway Firth (Table 5), and impacts on $\Delta\overline{|\tau_b|}$ are therefore more pronounced.

Impacts within the tidal lagoons themselves depend on impoundment bathymetry, hydraulic structure placement and the operation regime. Significant impacts on mean bed shear stress magnitude $\Delta\overline{|\tau_b|}$ occur in all impoundment areas (Section 4.5). In cases where the tidal lagoon is not situated in a previously high flow environment (SW, CO, LI and BL), portions of the impoundment experience both an increase and decrease in $\Delta\overline{|\tau_b|}$. A high overall decrease is experienced otherwise. Meanwhile, impoundment wetting and drying periods are shifted in a consistent manner as a result of the applied operation regime (Fig. 8). The exception is at LI, where both the phasing and magnitude of dry periods are notably altered. Each scheme is optimised to operate with pumping capabilities, here applied conservatively across every tidal cycle. Therefore, the manner in which LI acts as an outlier is a product of its shallower gradient at typical water elevation ranges (Fig. 3), making its intertidal zones more sensitive changes in tidal conditions.

5.4. Conversion of the tidal energy resource

CA and WA have a much lower 'Extraction Rate' (%) than all the other modelled schemes (Table 6). This suggests that the consistent impoundment design applied in this study contributes to their inefficient exploitation of the energy resource. An additional factor could be the rated head for the turbine being too small for the amplified tidal range at these tidal lagoon locations. Meanwhile, LI has the highest ambient resource $\overline{E_{A,yr}}$ ($\mathrm{GWh\ km^{-2}}$) of the Irish Sea lagoons, but extracts the lowest energy output E_{yr} (GWh/year). This is due to the highly intertidal zone LI encompasses, as discussed in Section 5.3. Constructing the embankment and turbine caissons over shallower regions could be advantageous, and an economic framework

is required to check if it is beneficial. These points all serve to highlight that whilst a consistent design provides a suitable platform for investigating power feasibility initially, tidal power lagoons require bespoke optimisation in later stages of planning.

SW and CA experience a significant drop in E_{yr} when all regional tidal lagoons are applied (Table 7). WA is much less affected, owing to its position within the channel. This observation contradicts Fig. 13, where the area surrounding WA is seen to experience a drop in $\overline{E_{\mathrm{A,yr}}}$ when all three lagoons are implemented. This can be attributed to discrepancies arising from power output prediction methods. The 2D model takes into account numerous additional variables compared to the ambient resource estimation. Hydrodynamics can thus be assumed to play an important role in the output estimation of this particular scheme. Power estimation discrepancies for different tidal power plants have been previously reported [27, 10]. Measures to mitigate the effects of cumulative impact on energy output could include implementing adaptive and complementary operation regimes [10, 14, 15]. Furthermore, magnified tidal currents resulting from tidal lagoons which impede tidal conditions could facilitate the feasibility of tidal stream energy developments. Energy output of the Irish Sea tidal lagoons is seen to be less affected by simultaneous operation of all regional schemes (Fig. 14 and Table 7).

A loss in energy output is consistently indicated in Table 7 between model configurations applying all tidal lagoons, and tidal lagoons in one region only. This emphasises that while impacts between the two regions are largely linear (Section 5.2), they can still be detected. This may be even more significant for larger schemes, and in particular tidal barrages. Future tidal power plant proposals must therefore consider their impact on subsequent constructions along the entire British west coast, and not just locally.

6. Conclusions

This study explores how siting and distribution of tidal power lagoons affects the nature of their hydro-environmental impacts. A consistent tidal energy lagoon design is applied in seven British west coast locations: three in the Bristol Channel and four in the Irish Sea. The use of a consistent design sheds light on the influence of regional characteristics on impacts and performance. The coastal flow solver *Thetis* is employed to simulate ambient tidal conditions. A representation of the presence and operation of combinations of the seven tidal energy lagoons is subsequently implemented, permitting quantification of tidal lagoon impacts. Individual and cumulative impacts related to harmonic tidal constituents, hydrodynamics, stratification, bed shear stress and tidal energy resource are explored. The following main conclusions can be drawn from the results and subsequent discussion:

- Numerical models representing large scale tidal lagoons must consider the spatial extent of their impacts when establishing boundary forcing locations. It is found that the open ocean boundaries in this study require placement up to or beyond the continental shelf.

- While impacts arising from the applied tidal power lagoon developments in the Bristol Channel and Irish Sea are detected in the other region (and consequently affect energy output), these impacts have a mostly linear relationship i.e. they can be summed when modelled separately.
- The constrained, estuarine coastline of the Bristol Channel leads to high tidal lagoon blockage, which in turn induces prominent individual and cumulative impacts throughout the region (including the energy conversion potential of other regional tidal power plants).
- The Irish Sea exhibits less constrained geometry, and as such, impacts of the tidal power plants it contains are more localised (generally in nearby bays and inlets), and combine little cumulatively.

Acknowledgements

L.M. would like to acknowledge the financial support of an EPSRC PhD studentship award, grant number EP/R513052/1(18-22). S.C.K. and M.D.P. acknowledge support from EPSRC under grants EP/M011054/1, EP/L000407/1, EP/R029423/1. A.A. acknowledges the support of NERC through the Industrial Innovation fellowship grant NE/R013209/2.

CRediT authorship contribution statement

Lucas Mackie: Conceptualization, Methodology, Validation, Formal Analysis, Investigation, Writing - original draft, Visualization. **Stephan C. Kramer:** Conceptualization, Writing - review & editing. **Matthew D. Piggott:** Conceptualization, Writing - review & editing, Supervision, Funding Acquisition. **Athanasios Angeloudis:** Conceptualization, Methodology, Investigation, Writing - review & editing, Supervision, Funding Acquisition.

References

[1] C. Baker, Tidal power, Energy Policy 19 (1991) 792–797.

[2] S. Waters, G. Aggidis, Tidal range technologies and state of the art in review, Renewable and Sustainable Energy Reviews 59 (2016) 514–529.

[3] D. Prandle, Simple theory for designing tidal power schemes, Advances in Water Resources 7 (1984) 21–27.

[4] S. P. Neill, A. Angeloudis, P. E. Robins, I. Walkington, S. L. Ward, I. Masters, M. J. Lewis, M. Piano, A. Avdis, M. D. Piggott, G. Aggidis, P. Evans, T. A. Adcock, A. Židonis, R. Ahmadian, R. Falconer, Tidal range energy resource and optimization – Past perspectives and future challenges, Renewable Energy 127 (2018) 763–778.

[5] Q. Ma, T. A. A. Adcock, Modification of tidal resonance in the Severn Estuary by a barrage and lagoon, Journal of Ocean Engineering and Marine Energy 6 (2020) 171–181.

[6] A. Angeloudis, R. Ahmadian, R. A. Falconer, B. Bockelmann-Evans, Numerical model simulations for optimisation of tidal lagoon schemes, Applied Energy 165 (2016) 522–536.

[7] L. Bernshtein, Tidal Energy for Electric Power Plants, Collection On Planning Hydro Developments Series Iv. Hydroelectric Power Plants, Designs And Materials, Israel Program for Scientific Translations, 1965. URL: https://books.google.co.uk/books?id=uf6ZuQEACAAJ.

[8] T. L. Shaw, M. J. Watson, Flexible power generation from the tides, Proceedings of the Institution of Civil Engineers - Engineering Sustainability 156 (2003) 119–123.

[9] G. Aggidis, D. Benzon, Operational optimisation of a tidal barrage across the Mersey estuary using 0-D modelling, Ocean Engineering 66 (2013) 69–81.

[10] A. Angeloudis, S. C. Kramer, A. Avdis, M. D. Piggott, Optimising tidal range power plant operation, Applied Energy 212 (2018) 680–690.

[11] R. Burrows, I. Walkington, N. Yates, T. Hedges, J. Wolf, J. Holt, The tidal range energy potential of the West Coast of the United Kingdom, Applied Ocean Research 31 (2009) 229–238. Renewable Energy: Leveraging Ocean and Waterways.

[12] G. Aggidis, O. Feather, Tidal range turbines and generation on the Solway Firth, Renewable Energy 43 (2012) 9–17.

[13] A. Angeloudis, M. D. Piggott, S. C. Kramer, A. Avdis, D. Coles, Comparison of 0-D , 1-D and 2-D model capabilities for tidal range energy resource assessments, in: 12th European Wave and Tidal Energy Conference, Cork, 2017, pp. 1–10. doi:https://doi.org/10.31223/osf.io/sjxf4.

[14] F. Harcourt, A. Angeloudis, M. D. Piggott, Utilising the flexible generation potential of tidal range power plants to optimise economic value, Applied Energy 237 (2019) 873–884.

[15] L. Mackie, D. Coles, M. Piggott, A. Angeloudis, The Potential for Tidal Range Energy Systems to Provide Continuous Power: A UK Case Study, Journal of Marine Science and Engineering 8 (2020).

[16] J. Xia, R. A. Falconer, B. Lin, Hydrodynamic impact of a tidal barrage in the Severn Estuary, UK, Renewable Energy 35 (2010) 1455–1468. Special Section: IST National Conference 2009.

[17] A. Cornett, J. Cousineau, I. Nistor, Assessment of hydrodynamic impacts from tidal power lagoons in the Bay of Fundy, International Journal of Marine Energy 1 (2013) 33–54.

[18] J. Zhou, S. Pan, R. A. Falconer, Effects of open boundary location on the far-field hydrodynamics of a Severn Barrage, Ocean Modelling 73 (2014) 19–29.

[19] A. Nekrasov, D. Romanenkov, Impact of tidal power dams upon tides and environmental conditions in the Sea of Okhotsk, Continental Shelf Research 30 (2010) 538–552. Tides in Marginal Seas - A special issue in memory of Prof Alexei Nekrasov.

[20] C. V. M. Vouriot, A. Angeloudis, S. C. Kramer, M. D. Piggott, Fate of large-scale vortices in idealized tidal lagoons, Environmental Fluid Mechanics 19 (2019) 329–348.

[21] T. Hooper, M. Austen, Tidal barrages in the UK: Ecological and social impacts, potential mitigation, and tools to support barrage planning, Renewable and Sustainable Energy Reviews 23 (2013) 289–298.

[22] K. Elliott, H. C. Smith, F. Moore, A. H. van der Weijde, I. Lazakis, Environmental interactions of tidal lagoons: A comparison of industry perspectives, Renewable Energy 119 (2018) 309–319.

[23] A. L. Baker, R. M. Craighead, E. J. Jarvis, H. C. Stenton, A. Angeloudis, L. Mackie, A. Avdis, M. D. Piggott, J. Hill, Modelling the impact of tidal range energy on species communities, Ocean & Coastal Management 193 (2020) 105221.

[24] J. Wolf, I. A. Walkington, J. Holt, R. Burrows, Environmental impacts of tidal power schemes, Proceedings of the Institution of Civil Engineers - Maritime Engineering 162 (2009) 165–177.

[25] N. Yates, I. Walkington, R. Burrows, J. Wolf, Appraising the extractable tidal energy resource of the UK's western coastal waters, Philosophical Transactions of the Royal Society A: Mathematical, Physical and Engineering Sciences 371 (2013) 20120181.

[26] T. Hooper, C. Hattam, A. Edwards-Jones, N. Beaumont, Public perceptions of tidal energy: Can you predict social acceptability across coastal communities in England?, Marine Policy 119 (2020) 104057.

[27] A. Angeloudis, R. A. Falconer, S. Bray, R. Ahmadian, Representation and operation of tidal energy impoundments in a coastal hydrodynamic model, Renewable Energy 99 (2016) 1103–1115.

[28] A. Angeloudis, R. A. Falconer, Sensitivity of tidal lagoon and barrage hydrodynamic impacts and energy outputs to operational characteristics, Renewable Energy 114 (2017) 337–351. Wave and Tidal Resource Characterization.

[29] J. K. Lundquist, K. K. DuVivier, D. Kaffine, J. M. Tomaszewski, Costs and consequences of wind turbine wake effects arising from uncoordinated wind energy development, Nature Energy 4 (2019) 26–34.

[30] S. Waldman, S. Weir, R. O'Hara Murray, D. Woolf, S. Kerr, Future policy implications of tidal energy array interactions, Marine Policy 108 (2019) 103611.

[31] T. Kärnä, S. C. Kramer, L. Mitchell, D. A. Ham, M. D. Piggott, A. M. Baptista, Thetis coastal ocean model: discontinuous Galerkin discretization for the three-dimensional hydrostatic equations, Geoscientific Model Development 11 (2018) 4359–4382.

[32] W. Pan, S. C. Kramer, M. D. Piggott, Multi-layer non-hydrostatic free surface modelling using the discontinuous Galerkin method, Ocean Modelling 134 (2019) 68–83.

[33] F. Rathgeber, D. A. Ham, L. Mitchell, M. Lange, F. Luporini, A. T. T. Mcrae, G.-T. Bercea, G. R. Markall, P. H. J. Kelly, Firedrake: Automating the Finite Element Method by Composing Abstractions, ACM Trans. Math. Softw. 43 (2016).

[34] T. Kärnä, B. de Brye, O. Gourgue, J. Lambrechts, R. Comblen, V. Legat, E. Deleersnijder, A fully implicit wetting–drying method for DG-FEM shallow water models, with an application to the Scheldt Estuary, Computer Methods in Applied Mechanics and Engineering 200 (2011) 509–524.

[35] A. Angeloudis, S. C. Kramer, N. Hawkins, M. D. Piggott, On the potential of linked-basin tidal power plants: An operational and coastal modelling assessment, Renewable Energy 155 (2020) 876–888.

[36] L. Mackie, P. S. Evans, M. J. Harrold, T. O'Doherty, M. D. Piggott, A. Angeloudis, Modelling an energetic tidal strait: investigating implications of common numerical configuration choices, Applied Ocean Research 108 (2021) 102494.

[37] N. Yates, I. Walkington, R. Burrows, J. Wolf, The energy gains realisable through pumping for tidal range energy schemes, Renewable Energy 58 (2013) 79–84.

[38] S. C. Endres, C. Sandrock, W. W. Focke, A simplicial homology algorithm for Lipschitz optimisation, Journal of Global Optimization 72 (2018) 181–217.

[39] P. Virtanen, R. Gommers, T. E. Oliphant, M. Haberland, T. Reddy, D. Cournapeau, E. Burovski, P. Peterson, W. Weckesser, J. Bright, S. J. van der Walt, M. Brett, J. Wilson, K. J. Millman, N. Mayorov, A. R. J. Nelson, E. Jones, R. Kern, E. Larson, C. J. Carey, İ. Polat, Y. Feng, E. W. Moore, J. VanderPlas, D. Laxalde, J. Perktold, R. Cimrman, I. Henriksen, E. A. Quintero, C. R. Harris, A. M. Archibald, A. H. Ribeiro, F. Pedregosa, P. van Mulbregt, SciPy 1.0 Contributors, SciPy 1.0: Fundamental Algorithms for Scientific Computing in Python, Nature Methods 17 (2020) 261–272.

[40] C. J. Mejia-Olivares, I. D. Haigh, A. Angeloudis, M. J. Lewis, S. P. Neill, Tidal range energy resource assessment of the gulf of california, mexico, Renewable Energy 155 (2020) 469–483.

[41] J. H. Simpson, J. R. Hunter, Fronts in the Irish Sea, Nature 250 (1974) 404–406.

[42] A. Angeloudis, Tidal range structure operation assessment and optimisation, Dams and Reservoirs 29 (2019) 45–54.

[43] S. Petley, G. Aggidis, Swansea Bay tidal lagoon annual energy estimation, Ocean Engineering 111 (2016) 348–357.

[44] C. Baker, P. Leach, G. B. D. of Trade, Industry, Tidal Lagoon Power Generation Scheme in Swansea Bay: A Report on Behalf of the Department of Trade and Industry and the Welsh Development Agency, DTI, 2006. URL: https://books.google.co.uk/books?id=R2QTMwEACAAJ.

[45] Tidal Lagoon Power, Ours to own: from first mover to mass manufacture. Building a new British industry from our natural advantage., 2016. URL: https://www.tidallagoonpower.com/wp-content/uploads/2016/09/Ours-to-Own_Tidal-Lagoon-Power_Oct-2016.pdf.

[46] P. Mohr, A. Lloyd, Levelised costs of power from tidal lagoons, Technical Report, Pöyry Management Consulting (UK) Ltd, UK, 2014.

[47] C. Hendry, The Role of Tidal Lagoons: Final Report, Technical Report, 2016. URL: https://hendryreview.files.wordpress.com/2016/08/hendry-review-final-report-english-version.pdf.

[48] The Crown Estate, UK Wave and Tidal: Key Resource Areas Project, Technical Report, The Crown Estate, 2012. URL: http://www.marineenergywales.co.uk/wp-content/uploads/2016/01/Summary-Report-FINAL.pdf.

[49] J. Xue, R. Ahmadian, O. Jones, R. A. Falconer, Design of tidal range energy generation schemes using a Genetic Algorithm model, Applied Energy 286 (2021) 116506.

[50] C. Binnie, A review of tidal power, 2019. URL: http://www.british-hydro.org/wp-content/uploads/2019/07/1.3-Binnie-C.pdf.

[51] Offshore Energy, LongBay SeaPower Plans to Build Large Tidal Lagoon (UK), 2014. [Online: https://www.offshore-energy.biz/longbay-seapower-plans-to-build-large-tidal-lagoon-uk/].

[52] Philippa Davey, Initial Project Meeting Note, 2014.

[53] C. Lyddon, A. Plater, J. Brown, T. Prime, J. Wolf, The impact of tidal lagoons on future flood risk on the North Wirral and Conwy coastline, UK, Technical Report, National Oceanography Centre, Southampton, 2015. URL: http://nora.nerc.ac.uk/id/eprint/512250/.

[54] North Wales Tidal Energy, North Wales presents a world-class site for a tidal lagoon, 2013. [Online: https://www.northwalestidalenergy.com/concept].

[55] UKAEA, Preliminary Survey of Small Scale Tidal Energy, Severn Tidal Power Report STP-4035 C, Technical Report, United Kingdom Atomic Energy Authority, London, 1984.

[56] BBC News, River Mersey tidal power plan granted £2.5m funding, 2020. [Online: https://www.bbc.co.uk/news/uk-england-merseyside-51677360].

[57] UKAEA, Preliminary Survey of Tidal Energy oF UK Estuaries, Severn Tidal Power Report STP-102, Technical Report, United Kingdom Atomic Energy Authority, London, 1980.

[58] G. D. Egbert, S. Y. Erofeeva, Efficient Inverse Modeling of Barotropic Ocean Tides, Journal of Atmospheric and Oceanic Technology 19 (01 Feb. 2002) 183 – 204.

[59] B. B. Parker, Tide Analysis and Prediction, National Oceanic and Atmospheric Administration, 2007. URL: https://tidesandcurrents.noaa.gov/publications/Tidal_Analysis_and_Predictions.pdf.

[60] NTSLF, Definitions of tidal levels and other parameters, 2021. URL: https://www.ntslf.org/tgi/definitions.

[61] BODC, UK Tide Gauge Network Data, 2017. URL: https://www.bodc.ac.uk/data/hosted_data_systems/sea_level/uk_tide_gauge_network/processed/.

[62] C. Garrett, D. Greenberg, Predicting changes in tidal regime: The open boundary problem, Journal of Physical Oceanography 7 (1977) 171 – 181.

[63] A. Avdis, A. S. Candy, J. Hill, S. C. Kramer, M. D. Piggott, Efficient unstructured mesh generation for marine renewable energy applications, Renewable Energy 116 (2018) 842–856.

[64] C. Geuzaine, J.-F. Remacle, Gmsh Reference Manual, 2020. URL: https://gmsh.info/.

[65] Digimap, Marine Digimap, 2020. URL: https://digimap.edina.ac.uk/marine.

[66] GEBCO, GEBCO Gridded Bathymetry Data, 2020. URL: https://www.gebco.net/data_and_products/gridded_bathymetry_data/.

[67] J. Horrillo-Caraballo, Y. Yin, I. Fairley, H. Karunarathna, I. Masters, D. Reeve, A comprehensive study of the tides around the Welsh coastal waters, Estuarine, Coastal and Shelf Science (2021) 107326.

[68] S. C. Warder, M. D. Piggott, Optimal experiment design for bottom friction parameter estimation, EarthArXiv (2020).

[69] L. Mackie, F. Harcourt, A. Angeloudis, M. D. Piggott, Income optimisation of a fleet of tidal lagoons, in: 13th Wave and Tidal Energy Conference, Naples, 2019, pp. 1–10. doi:https://www.researchgate.net/publication/335686602_Income_optimisation_of_a_fleet_of_tidal_lagoons.

[70] E. Chappuis, M. Terradas, M. E. Cefalì, S. Mariani, E. Ballesteros, Vertical zonation is the main distribution pattern of littoral assemblages on rocky shores at a regional scale, Estuarine, Coastal and Shelf Science 147 (2014) 113–122.

[71] F. Daidu, W. Yuan, L. Min, Classifications, sedimentary features and facies associations of tidal flats, Journal of Palaeogeography 2 (2013) 66–80.

[72] C. Gao, T. A. A. Adcock, On the Tidal Resonance of the Bristol Channel, International Journal of Offshore and Polar Engineering 27 (2017) 177–183.

[73] S. W. Fong, N. S. Heaps, Note on Quarter Wave Tidal Resonance in the Bristol Channel, 1978. URL: http://nora.nerc.ac.uk/id/eprint/11127/, i.O.S. Report No. 63.